

**A NEAR FIELD, NON-CONTACT VIBRATION DETECTOR USING
GIANT MAGNETORESISTANCE SENSORS**

A Dissertation
Presented to
The Academic Faculty

by

Peter Wahba Mickael

In Partial Fulfillment
of the Requirements for the Degree
Master of Science in the
School of Electrical and Computer Engineering

Georgia Institute of Technology
December 2018

COPYRIGHT © 2018 BY PETER MICKAEL

**A NEAR FIELD, NON-CONTACT VIBRATION DETECTOR USING
GIANT MAGNETORESISTANCE SENSORS**

Approved by:

Dr. James S Kenney, Advisor
School of Electrical and Computer Engineering
Georgia Institute of Technology

Dr. William D Hunt
School of Electrical and Computer Engineering
Georgia Institute of Technology

Dr. Aaron D Lanterman
School of Electrical and Computer Engineering
Georgia Institute of Technology

Date Approved: December 7, 2018

ACKNOWLEDGEMENTS

I would like to thank Dr. Kenney for his guidance and advice throughout the research process. I would also like to thank Lucas Wray for his assistance with the signal processing in gathering the results. Lastly, I would like to thank my parents, Medhat and Sonia, my brother, Andrew, and all my family and friends for their continuous support.

TABLE OF CONTENTS

ACKNOWLEDGEMENTS	iv
LIST OF TABLES	vii
LIST OF FIGURES	viii
LIST OF SYMBOLS AND ABBREVIATIONS	x
SUMMARY	xi
CHAPTER 1. Introduction	1
1.1 Natural and Damped Vibrations	1
1.2 Methods of Detecting Vibration	3
1.2.1 Contact Vibration Sensors	3
1.2.2 Non-contact Vibration Sensors	10
1.2.3 Comparison of Sensors	15
CHAPTER 2. GMR Sensors and Applications	19
2.1 Magnetoresistive Sensors	19
2.1.1 AMR Sensors	19
2.1.2 GMR Sensors	20
2.1.3 TMR Sensors	21
2.1.4 Comparison of MR Sensors	21
2.2 Applications of GMR Sensors	22
2.2.1 MRAM	22
2.2.2 Crankshaft Position Sensors	23
2.3 GMR Sensors as Vibration Detectors	24
CHAPTER 3. String Vibrations	29
3.1 The Wave Equation	29
3.2 The Plucked String	31
3.2.1 Harmonic Amplitudes	32
CHAPTER 4. GMR Sensors as Electric Guitar Pickups	35
CHAPTER 5. Experimental Results	37
5.1 Sensor Characteristics	37
5.2 Circuit Design and Testing Setup	38
5.3 Results	40
5.3.1 GMR Sensor Placed Near Neck Pickup	43
5.3.2 GMR Sensor Placed Near Bridge Pickup	49
5.3.3 Conclusions	55
CHAPTER 6. Conclusion	57

LIST OF TABLES

Table 1 – Comparison of Different Sensors Used for Vibration	18
Table 2 – Evolution of MR Sensors	21
Table 3 – GMR Amplitudes for String Plucked at 1/4 Length (Neck)	44
Table 4 – Inductive Pickup Amplitudes for String Plucked at 1/4 Length	44
Table 5 – GMR Amplitudes for String Plucked at 1/3 Length (Neck)	46
Table 6 – Inductive Pickup Amplitudes for String Plucked at 1/3 Length	46
Table 7 – GMR Amplitudes for String Plucked at 1/2 Length (Neck)	48
Table 8 – Inductive Pickup Amplitudes for String Plucked at 1/2 Length	48
Table 9 – GMR Amplitudes for String Plucked at 1/4 Length (Bridge)	50
Table 10 – Inductive Pickup Amplitudes for String Plucked at 1/4 Length	50
Table 11 – GMR Amplitudes for String Plucked at 1/3 Length (Bridge)	52
Table 12 – Inductive Pickup Amplitudes for String Plucked at 1/3 Length	52
Table 13 – GMR Amplitudes for String Plucked at 1/2 Length (Bridge)	54
Table 14 – Inductive Pickup Amplitudes for String Plucked at 1/2 Length	54

LIST OF FIGURES

Figure 1 – Effect of damping on Vibrations	3
Figure 2 – Frequency response of piezoelectric accelerometers	6
Figure 3 – Compressional, shear, and flexural accelerometers	6
Figure 4 – Typical IEPE accelerometer	6
Figure 5 – Silicon resistors bonded to accelerometer fixture	8
Figure 6 – Typical capacitive accelerometer	9
Figure 7 – Modulator-demodulator circuit	10
Figure 8 – A common LDV setup	11
Figure 9 – Single-coil vs humbucker pickups	13
Figure 10 – Typical capacitive displacement sensor	14
Figure 11 – LC oscillator used in an eddy-current probe	14
Figure 12 – Hall effect sensor	15
Figure 13 – Temperature dependence of GMR and Hall effect sensors	17
Figure 14 – AMR characteristics	19
Figure 15 – GMR structures	20
Figure 16 – TMR structure	21
Figure 17 – Early MRAM concept	22
Figure 18 – Air gaps attained with different magnetic sensors	24
Figure 19 – Block diagram of GMR vibration detector	26
Figure 20 – Spectrum of drill bits at 4700 and 8500 rpm	26
Figure 21 – Spectrum of well-aligned and misaligned drill bit	27
Figure 22 – Spectrum of 440 Hz tuning fork (3-axis)	27
Figure 23 – Spectrum of machinery fault simulator	28

Figure 24 – Spectrum of 440 Hz tuning fork (single-axis)	28
Figure 25 – Ideal string model harmonic spectrum	34
Figure 26 – Inductive pickup and GMR response to 50 Hz mains hum	35
Figure 27 – Inductive pickup and GMR response to 5 kHz external field	35
Figure 28 – Comparison of GMR, inductive, and Hall effect pickups	36
Figure 29 – GMR half-bridge setup	37
Figure 30 – NVE AA-005 sensor characteristics	38
Figure 31 – Bridge amplifier circuit	39
Figure 32 – String vibration setup	40
Figure 33 – Time domain plot of GMR output	42
Figure 34 – Time domain plot of inductive pickup output	42
Figure 35 – Spectrum of GMR and inductive pickup for 1/4 string pluck (neck)	43
Figure 36 – Spectrum of GMR and inductive pickup for 1/3 string pluck (neck)	45
Figure 37 – Spectrum of GMR and inductive pickup for 1/2 string pluck (neck)	47
Figure 38 – Spectrum of GMR and inductive pickup for 1/4 string pluck (bridge)	49
Figure 39 – Spectrum of GMR and inductive pickup for 1/3 string pluck (bridge)	51
Figure 40 – Spectrum of GMR and inductive pickup for 1/2 string pluck (bridge)	53

LIST OF SYMBOLS AND ABBREVIATIONS

PE	Piezoelectric
IEPE	Internal Electronic Piezoelectric
LDV	Laser Doppler Vibrometer
MR	Magnetoresistance
AMR	Anisotropic Magnetoresistance
GMR	Giant Magnetoresistance
TMR	Tunnel Magnetoresistance

SUMMARY

Giant magnetoresistance (GMR) sensors are explored for their use in detecting vibrations. GMR sensors have been widely used in magnetoresistive random-access memory (MRAM), and they have the potential to be utilized in many other industries due to their small size and low power consumption.

A summary of sensors and transducers used for vibration measurements is given. In addition, an investigation of string vibrations is discussed as the GMR sensors were tested against traditional inductive electric guitar pickups.

GMR sensors show a distinct advantage for measuring string vibrations. The GMR device gives an output related to the position of the moving string as opposed to its velocity and displays a flat frequency response. The harmonic spectrum produced is a truer representation of the string dynamics as there is no frequency response introduced by the sensor itself.

CHAPTER 1. INTRODUCTION

Vibration is a mechanical phenomenon in which oscillations occur around an equilibrium point. Vibrations can be both desirable and undesirable. For instance, vibrations are the basis of sound and are essential in the workings of all musical instruments. On the other hand, vibrations of a particular frequency can indicate a fault in a system or component, as can be seen commonly in automobiles. In any case, it is essential to sense these vibrations as they are prevalent in essentially every industry.

1.1 Natural and Damped Vibrations

Vibrations of mechanical systems can be categorized most simply in two characteristics: whether the vibration is free or forced, and the amount of damping in the system. In the most general case, a vibrating system can be modeled by a second order linear system with mass M , damping coefficient D , stiffness K , and external force F :

$$M \frac{d^2x}{dt^2} + D \frac{dx}{dt} + Kx = F \quad (1.1)$$

A free vibration is one in which no external force acts on the body in order to keep it in motion (e.g. $F = 0$). The vibration is excited by some initial displacement and is left to vibrate at its natural frequency [1]. An example of free vibration is a plucked guitar string: the plucking motion initiates the vibration and the frequency is determined by the nature of the string (e.g. tension, mass, length, etc.). The natural frequency, ω_n , is defined as:

$$\omega_n = \sqrt{\frac{K}{M}} \quad (1.2)$$

The damping of a vibrating system describes the amount of friction that acts to dissipate the energy of the system. Systems can be described as undamped, underdamped, critically-damped, or overdamped. Undamped systems oscillate indefinitely at a constant amplitude. Underdamped systems oscillate with a decreasing amplitude until they eventually come to rest. Critically-damped and overdamped systems both return to equilibrium without oscillating. The difference between the two is that critically-damped systems return to equilibrium in the minimum amount of time. The amount of damping in a system is best described by the damping ratio, ζ . The damping ratio is given by:

$$\zeta = \frac{D}{2\sqrt{KM}} \quad (1.3)$$

This ratio varies from undamped ($\zeta = 0$), underdamped ($\zeta < 1$), critically-damped ($\zeta = 1$), and overdamped ($\zeta > 1$). It can be seen from Figure 1 that as ζ increases from zero, the oscillation amplitude decreases at a faster rate. If ζ goes above one, the signal does not overshoot, but takes longer to reach equilibrium than the critically-damped case ($\zeta = 1$). Equation (1.1) can be rewritten to include ω_n and ζ as follows:

$$\frac{d^2x}{dt^2} + 2\zeta\omega_n \frac{dx}{dt} + \omega_n^2 x = \frac{F}{M} \quad (1.4)$$

In addition to altering the amplitude of vibration, the damping ratio also shifts the frequency of vibration. The new frequency is called the *damped natural* frequency:

$$\omega_d = \omega_n \sqrt{1 - \zeta^2} \quad (1.5)$$

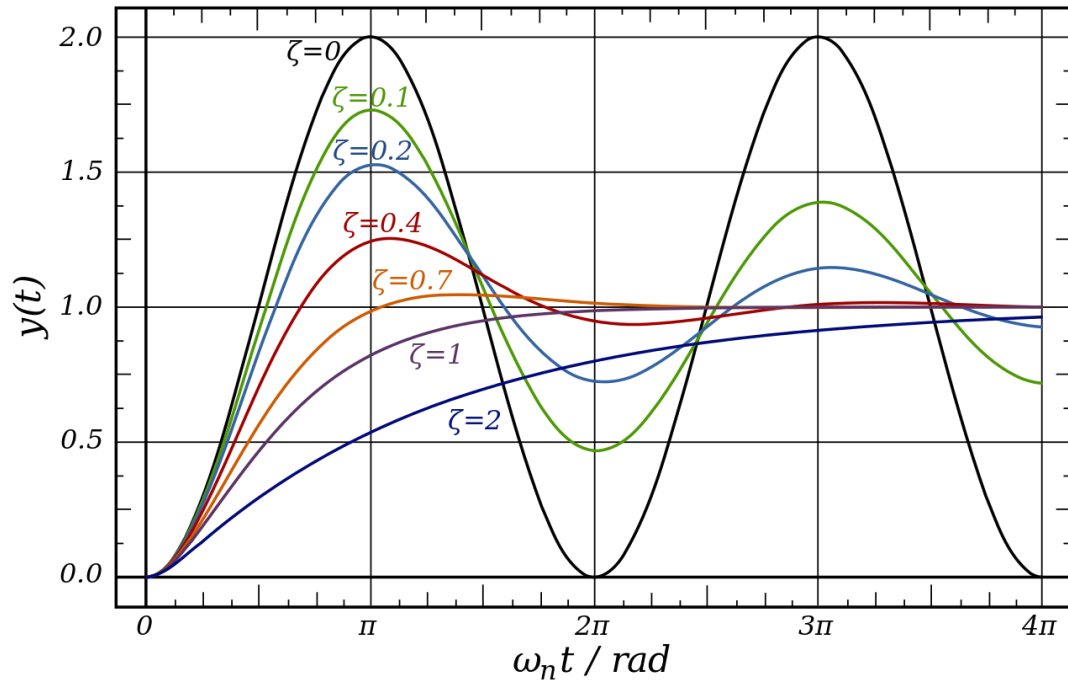


Figure 1: Effect of damping on vibrations

A forced vibration, on the other hand, relies on a disturbing force to keep the body vibrating [1]. The vibration of a building due to an earthquake is an example of a forced vibration. The amplitude and frequency of the vibrations are determined by the earthquake and not the building itself. Fault conditions in machines can commonly be characterized by forced vibrations.

1.2 Methods of Detecting Vibration

1.2.1 Contact Vibration Sensors

There are a variety of sensors classically used for a contact vibration measurement, including piezoelectric, piezoresistive, and capacitive accelerometers.

1.2.1.1 Piezoelectric Accelerometers

Piezoelectric accelerometers use materials which provide an electrical output proportional to the mechanical stress applied. This effect was first discovered by J. and P. Curie in 1880. Their knowledge of pyroelectricity (electric potential due to temperature change) combined with their research of crystal structures led to the discovery of piezoelectricity in quartz and other crystals.

The piezoelectric element in a sensor acts as a spring (with stiffness k) which connects the base of the sensor to a seismic mass. The sensor uses Newton's second law of motion ($F = ma$) to provide an output related to acceleration. The frequency response of the sensor is governed by its resonant frequency, $\omega = \sqrt{k/m}$. The sensors display a generally flat frequency response at frequencies below this resonant frequency, as can be seen in Figure 2 [2].

Compression mode sensors sandwich the sensing element in between a mounting base and seismic mass. Shear mode sensors, similarly, sandwich the sensing material in between a center post and some seismic mass. Flexural mode sensors use beam-shaped sensing materials, usually quartz. The material is supported by some mass which creates a strain when accelerated. Flexural sensors are insensitive to transverse motion. These configurations can be seen in Figure 3 [2].

Most piezoelectric accelerometers contain built-in signal conditioning circuitry. This circuitry converts the high-impedance charge signal from the piezoelectric element into a low-impedance voltage signal that can be easily transmitted via two-wire or coaxial cable [2]. These sensors are called internal electronic piezoelectric, or IEPE, accelerometers. For

most applications, IEPE sensors are favorable. The alternative to IEPE accelerometers are charge-mode sensors, which provide a high-impedance output charge signal. These sensors are generally used when operating temperatures exceed the usable limits of the internal circuitry of IEPEs [2].

Piezoelectric sensors commonly use either quartz or man-made ceramics. Quartz is a crystal which is naturally piezoelectric and does not relax into another state. Quartz crystals are also very stable over temperature, which makes them very advantageous for many industrial applications. Ceramics, such as aluminum nitride (AlN), zinc oxide (ZnO), and now most commonly lead zirconated titanate ($\text{Pb}[\text{Zr}_x\text{Ti}_{1-x}]\text{O}_3$), are forced to be piezoelectric by a process called “poling”. This process exposes the material to a high intensity electric field. This aligns the electric dipoles, making the material piezoelectric [2]. Quartz is predominately used in voltage-amplified systems as it has a high voltage sensitivity when compared to ceramic materials. Conversely, ceramics are used in charge-amplified systems as they have higher charge sensitivity when compared to quartz [2].

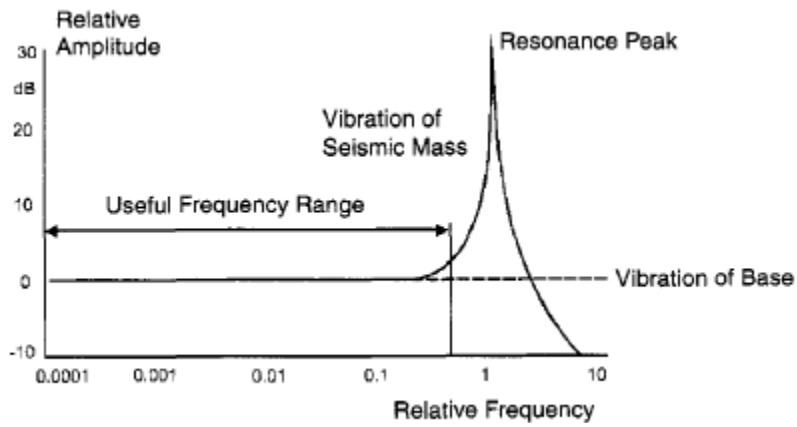


Figure 2: Frequency response of piezoelectric accelerometers

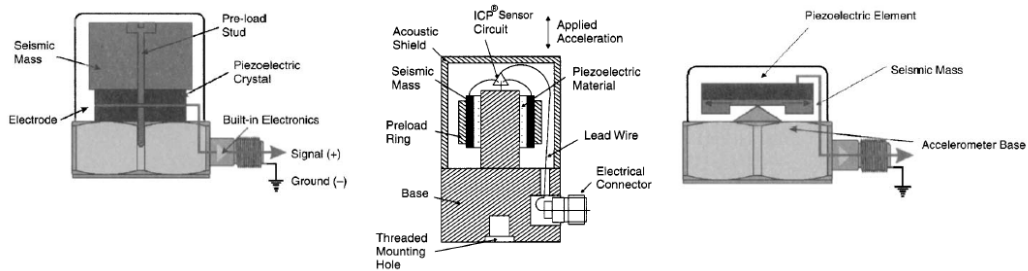


Figure 3: From left to right: compressional, shear, and flexural mode accelerometers

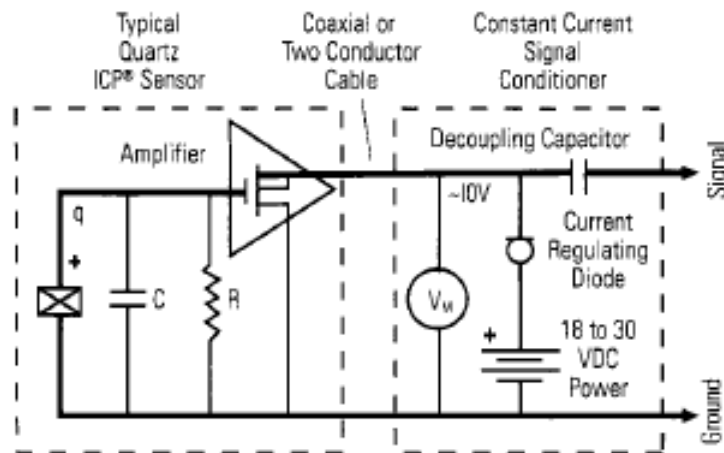


Figure 4: Typical IEPE accelerometer circuit

1.2.1.2 Piezoresistive Accelerometers

Piezoresistive sensors use a change in electrical resistance under strain to produce an electrical output. Lord Kelvin first discovered the effect in 1856, and the large piezoresistive effect was discovered in semiconductors in 1954 by C.S. Smith.

A material's piezoresistivity (i.e. its change in resistance with applied force) is described by its gauge factor:

$$\text{Gauge Factor} = \frac{\Delta R/R}{\Delta L/L} = \frac{\Delta R/R}{\xi} \quad (1.6)$$

The $\Delta L/L$ term describes the applied strain. This strain can be related to the applied force by the Young's modulus of the material, which is a measure of its stiffness:

$$\text{Young's modulus, } E = \frac{\text{Stress}}{\text{Strain}} = \frac{\sigma}{\xi} \quad (N/m^2) \quad (1.7)$$

Semiconductor materials possess very high gauge factors which make them popular choices for piezoresistors, with *p*-type and *n*-type silicon exhibiting gauge factors of +200 and -125 respectively [3]. Bulk silicon resistors are commonly configured in a Wheatstone bridge configuration and fixed to the accelerometer as shown in Figure 5 [2]. Silicon also exhibits high stiffness, with a Young's modulus of approximately 190 GPa (1 Pa = 1 N/m²). Piezoresistive accelerometers are manufactured such that silicon is both the flexural and transduction element. This is advantageous as the high stiffness of silicon results in a higher resonant frequency [2]. A major disadvantage of this method is the temperature coefficient

of resistance of semiconductor materials. Semiconductors display a temperature coefficient of resistance which is exponential, as opposed to linear in conductors.

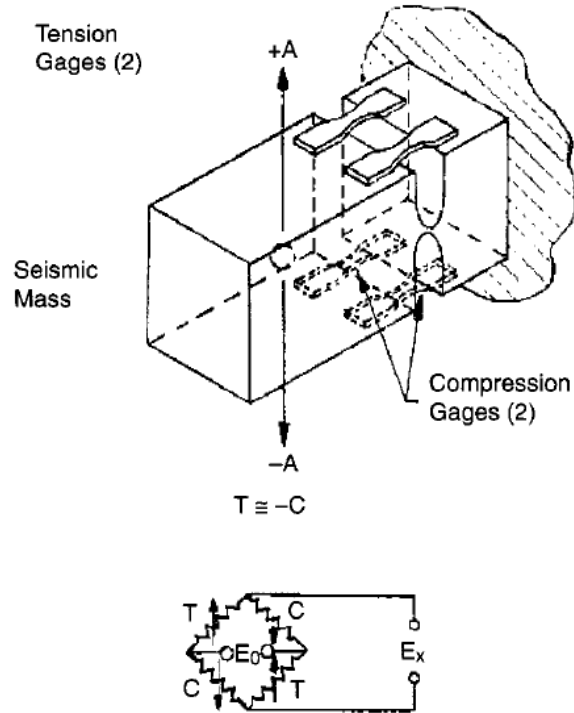


Figure 5: Silicon resistors bonded to accelerometer fixture

1.2.1.3 Capacitive Accelerometers

Capacitive accelerometers, as the name suggests, use a change in capacitance to represent acceleration. In its simplest form, the sensor consists of a fixed electrode and a moving electrode separated by some distance of dielectric material. A common type of capacitive accelerometer can be seen in Figure 6 [2].

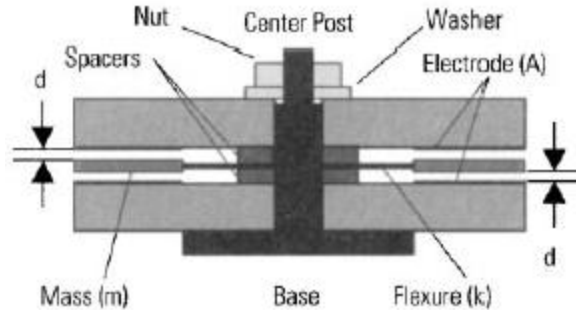


Figure 6: Typical capacitive accelerometer

In this design, the electrodes share a moving diaphragm. The diaphragm, or flexure, has mass m and stiffness k . When the sensor experiences an acceleration, the spring-mass experiences a force ($F = ma$). This force causes the spring-mass to deflect according to Hooke's law:

$$X = \frac{F}{k} \quad (1.8)$$

The deflection, X , of the spring mass causes the distance between the electrodes and the diaphragm to vary [2]. The changing capacitance values are described as follows:

$$C = \frac{A\epsilon_0\epsilon_r}{d \pm X} \quad (1.9)$$

A represents the surface area of the electrodes, d represents the distance between the spring-mass and each electrode, and ϵ_0 and ϵ_r are the permittivity of free space and relative permittivity of the dielectric separating the plates respectively.

In order to convert this change in capacitance to a usable voltage signal, a modulator-demodulator circuit or its equivalent is typically used. This circuit consists of an oscillator and bridge of capacitors, with two capacitors changing value in accordance with the acceleration of the system. The bridge network serves as a divider which causes the

oscillator amplitude to vary with the changes in capacitance. These signals are then rectified and summed together. The resultant output is then amplified and filtered to remove any jitter cause by the oscillator. A typical circuit can be seen in Figure 7 [2].

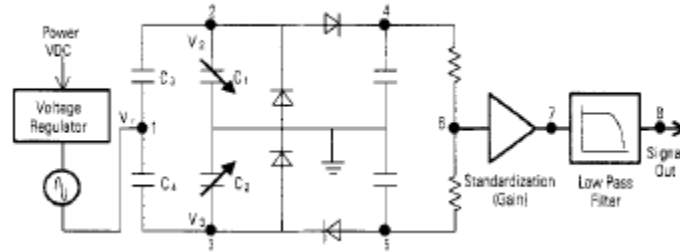


Figure 7: Modulator-demodulator circuit

1.2.2 Non-contact Vibration Sensors

1.2.2.1 Laser Doppler Vibrometers

The working principle of the LDV, as the name suggests, is the Doppler effect. This effect describes the relative change in wavelength (and frequency) of a wave when the distance between the source and observer is changing. The observed frequency is:

$$f_{observed} = f_{source} \left(\frac{c}{c \pm v} \right) \quad (1.10)$$

In this case of LDVs, the velocity of the object is denoted as v (as the source is considered to be stationary), and the speed of light is denoted as c . If the object is approaching the source, the minus sign is taken in the denominator and the frequency increases. The opposite is true if the observer is moving away from the source [4]. The equation can be expanded as follows to denote the frequency shift (or the Doppler frequency):

$$f_{observed} = f_{source} \left(\frac{c}{c \pm v} \right) \approx f_{source} \left(\frac{c \mp v}{c} \right) = f_{source} + f_{Doppler} \quad (1.11)$$

The LDV uses a laser, which emits light at a certain frequency, and detects the frequency shift of the reflected of the reflected light. Therefore, the Doppler shift must be taken twice:

$$f_{Doppler} = 2 \frac{v}{\lambda_{source}} \quad (1.12)$$

The frequency of the light emitted from the laser is very high (usually greater than 10^{14} Hz) and thus cannot be demodulated directly to obtain the Doppler shift. To obtain the Doppler shift (and the corresponding velocity), the interference between the source light and reflected light is observed [4]. This is typically done using an optical interferometer, shown in Figure 8 [4]. This interferometer uses a beam-splitter and a photodetector which responds to the difference frequency (or beat frequency) of the two waves it sees [4]. This beat frequency is the Doppler shift.

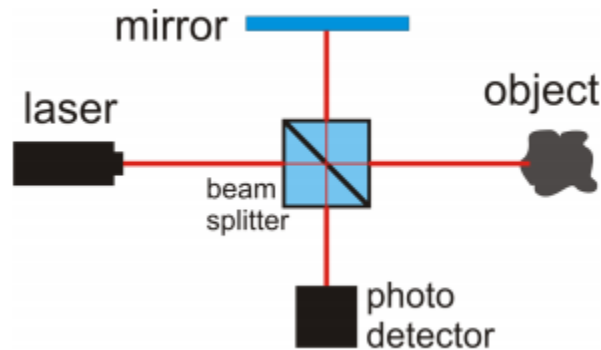


Figure 8: A common LDV setup

1.2.2.2 Variable Reluctance Sensors

Variable reluctance sensors work on the principle of Faraday's law of induction. For a single wire loop, Faraday's law states that a changing magnetic flux will produce an electromotive force (EMF) through the loop. For a tightly wound coil with N turns, Faraday's law states:

$$\varepsilon = -N \frac{d\Phi_B}{dt} \quad (1.13)$$

ε is the EMF in volts, and Φ_B is the magnetic flux through a single loop of wire.

The most prevalent variable reluctance sensor is undoubtedly the magnetic guitar pickup. The magnetic pickup, in its most general use, consists of a permanent magnet (usually made from alnico or ferrite) wrapped with a coil of wire with several thousand turns. As the string (made of steel or other ferromagnetic materials) is plucked, its vibration disturbs the magnetic field created by the permanent magnet. This creates a time-varying magnetic flux which induces a voltage in the coil. This voltage is then sent to an audio amplifier and subsequent loudspeaker.

Single-coil pickups have a major disadvantage in that they are susceptible to magnetic interference from nearby electronics, such as mains power hum. In an effort to overcome this, the "humbucking" or "humbucker" pickup was invented. This pickup uses two separate coils wound in reverse to one another, with the magnetic poles in each coil opposite in each winding to produce a differential output. The ambient noise enters the coils as a common-mode signal and is cancelled out due to the windings being reversed. The guitar signal, however, is added in-phase from each pickup. This is due to the fact that

the windings are reversed and the pole pieces having opposite polarity. This, in effect, doubles the voltage signal from each guitar string.

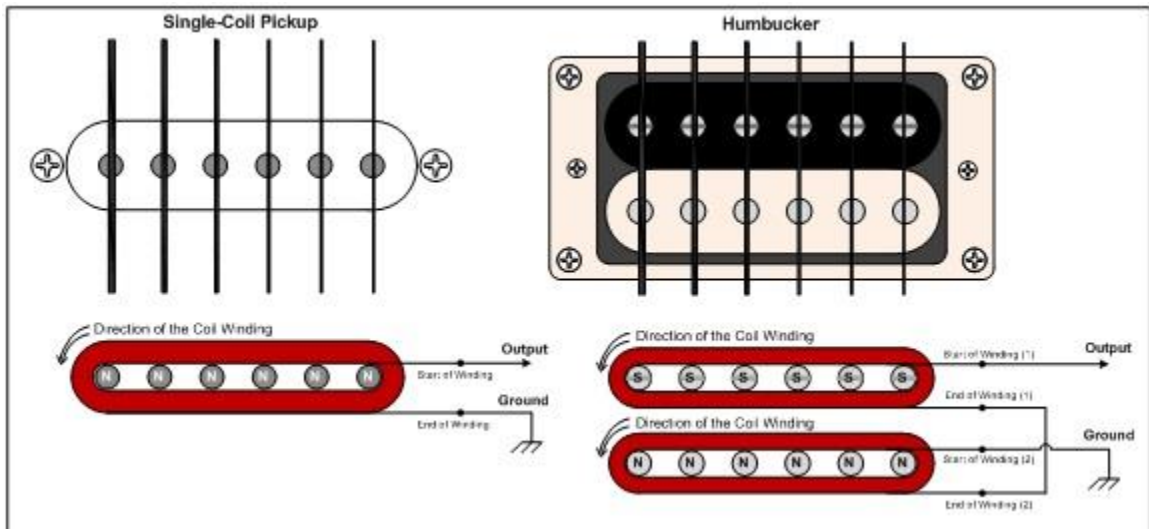


Figure 9: Single-coil vs humbucker pickup

1.2.2.3 Capacitive Displacement Sensors

Capacitive displacement sensors use the vibrating target as one plate of the capacitor, with the other plate being a stationary capacitive probe. The movement of the target causes the distance between the plates to change, thus changing the capacitance. Capacitive displacement sensors differ from capacitive accelerometers in that the freely moving target directly causes the distance of the plates to change, rather than the acceleration inducing a force in a spring-mass. Capacitive displacement sensors also provide a non-contact measurement, which can be beneficial in many applications.

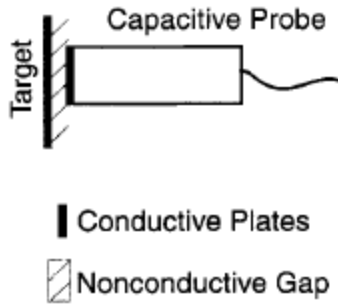


Figure 10: Typical capacitive displacement sensor

1.2.2.4 Inductive Displacement Sensors

Inductive displacement sensors, also called eddy-current sensors, use electromagnetic (EM) fields to induce a current in a conductive target. This field is generated by a coil fed by an oscillator, usually tuned by a parallel capacitor [5]. The current induced in the target generates an EM field of its own, which changes the effective coil inductance. This change in inductance changes the resonant frequency of the LC tank circuit.

The permeability of ferromagnetic targets will simultaneously increase the effective inductance of the coil as the probe gets closer to the target as the field generated decreases the inductance [5]. These opposing changes can be difficult to characterize. An ideal target for eddy-current sensors are materials like Aluminum, which are conductive but not ferromagnetic.

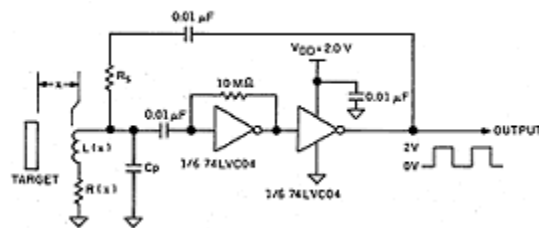


Figure 11: LC oscillator used in an eddy-current probe

1.2.2.5 Hall Effect Sensors

Hall effect sensors produce a voltage output in response to an applied magnetic field. Discovered by Edwin Hall in 1879, the Hall effect is the production of a voltage across an electric conductor in the presence of a magnetic field when a current is sent across its length. The electrons moving through the magnetic field experience a Lorentz force which creates the voltage, known as the Hall voltage. This voltage is illustrated in Figure 12 [6]. This effect is amplified in semiconductors, and most Hall effect sensors are made of III-V semiconductor indium antimonide (InSb) [6].

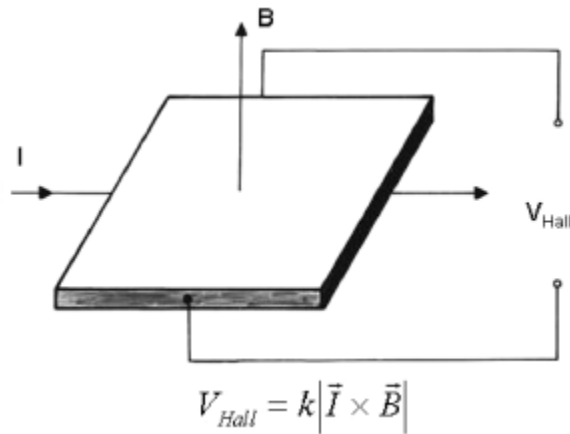


Figure 12: Hall effect sensor

1.2.3 *Comparison of Sensors*

Contact vibration sensors have a distinct advantage in that they are not restricted by the material of the vibrating structure. IEPE accelerometers are easier to implement and are more precise than charge-mode accelerometers, however charge-mode sensors are much more reliable at high temperatures. Piezoresistive and capacitive accelerometers generally have lower sensitivities when compared to piezoelectric sensors, however they both have a true DC response whereas piezoelectric sensors do not. Piezoresistive sensors

are highly linear when compared to capacitive sensors, but they also have very high temperature coefficients [2].

The main drawback in using contact sensors for vibration measurement is that, namely, they have to be mounted to the vibrating structure in order to provide an accurate reading. This cannot be afforded in some applications where the sensor cannot be in contact with the vibrating structure due to weight or other concerns. For these applications, velocity and position sensors are used.

LDVs are extremely accurate devices and can sense vibrations over 1 MHz. The drawback is their extremely high cost and size when compared to other miniature sensors. Variable reluctance sensors are extremely durable as all components are passive. They do not require an external power supply or circuitry to operate reliably, and this has made them a common choice in rough and high temperature environments (such as the automotive industry). Variable reluctance sensors, however, favor higher frequency vibrations [9].

Measuring displacement has an advantage over measuring velocity as the sensors display a *flat* frequency response. Variable reluctance sensors, for instance, essentially amplify higher frequency vibrations due to their operating principle. This imbalance in frequency response can skew the spectrum produced by the vibration and lead to inaccurate results and conclusions. Displacement sensors do not show a similar dependence on frequency.

Capacitive and inductive (eddy-current) displacement sensors have been traditionally used to measure vibration. These sensors, however, are orders of magnitude larger than

solid state magnetic sensors, such as Hall effect and magnetoresistive (to be discussed in more detail in Chapter 2). Hall effect sensors offer a smaller size alternative, however recent discoveries in magnetoresistive (MR) sensors have made MR sensors more favorable in many applications. In general, MR sensors display higher frequency responses, higher sensitivities, and operate more reliably over temperature when compared to Hall effect sensors [2].

A comparison of different sensors can be seen in Table 1.

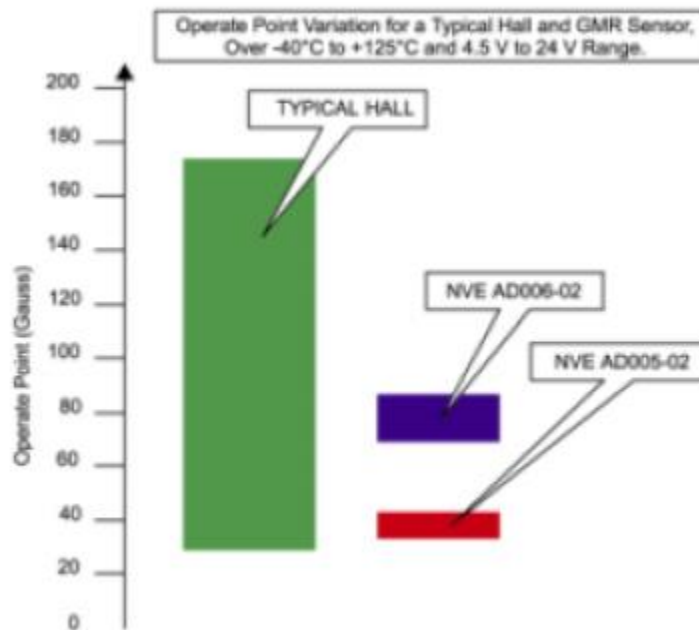


Figure 13: Temperature dependence of GMR and Hall effect sensors (Source: Rhopoint Components)

Table 1: Comparison of Different Sensors Used for Vibration

Sensor	Measurement	Contact / Non-contact	Sensitivity/ Resolution	Bandwidth
IEPE	Acceleration	Contact	High	~50 kHz
Charge Mode PE	Acceleration	Contact	High	~50 kHz
Piezoresistive	Acceleration	Contact	Low	~10 kHz
Capacitive Accelerometer	Acceleration	Contact	Average	~1 kHz
LDV	Velocity	Non-contact	Very High	> 1 MHz
Variable Reluctance	Velocity	Non-contact	High	~100 kHz
Capacitive Displacement	Displacement	Non-contact	Average	~10 kHz
Inductive (eddy-current)	Displacement	Non-contact	Average	~100 kHz
Hall Effect	Displacement	Non-contact	Average	~ 20 kHz
Magnetoresistive	Displacement	Non-contact	High	~ 100 kHz

CHAPTER 2. GMR SENSORS AND APPLICATIONS

2.1 Magneto-resistive Sensors

Magneto-resistive sensors use a change in electrical resistance due to an external magnetic field. These resistors are usually arranged in a Wheatstone bridge configuration to provide an output voltage proportional to magnetic field strength. There are multiple types of MR sensors, with the most popular being anisotropic magnetoresistance (AMR), giant magnetoresistance (GMR), and tunnel magnetoresistance (TMR) sensors.

2.1.1 AMR Sensors

Materials such as permalloy (80% nickel and 20% iron), exhibit anisotropic magnetoresistance. This is a phenomenon in which the electrical resistance of the material is dependent on the angle between magnetization and current flow. The resistance of the AMR material is lowest when the magnetization is perpendicular to the direction of current flow [6]. This can be seen in Figure 13. AMR sensors can show changes in resistance up to 4%.

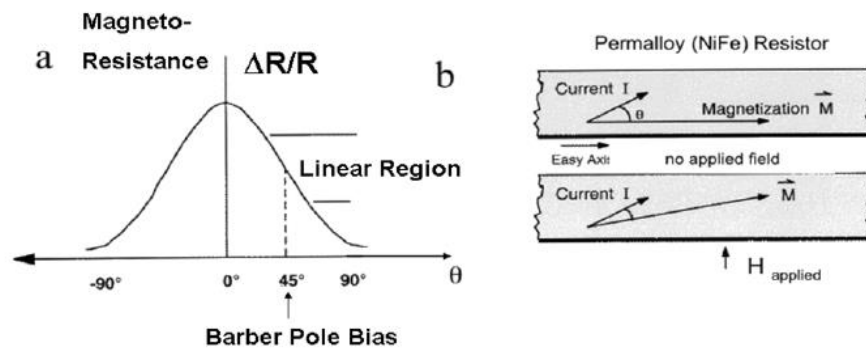


Figure 14: AMR characteristics (a) change in resistance vs. angle between magnetization and direction of current flow, (b) change in angle due to external magnetic field

2.1.2 GMR Sensors

A bigger change in resistance can be seen in the giant magnetoresistance effect. This effect was discovered independently by Albert Fert and Peter Grünberg in 1988. They were both awarded the Nobel Prize in Physics in 2007 for their discovery. The simplest GMR structure is the spin valve, which consists of two ferromagnetic metal layers separated a nonferromagnetic conductor. One of the ferromagnetic layers is “pinned” with an antiferromagnetic layer [5]. This pinning layer restricts one of the magnetic layers from responding to an external field. The resistance of the total stack is lowest when the magnetizations of the layers are parallel, and highest when antiparallel.

Most modern GMR sensors, however, are made in a multilayer structure where the pinning layer is removed. The thickness of the nonferromagnetic layer is adjusted to couple the ferromagnets antiferromagnetically. This results in a greater resistance change. Spin valve and multilayer GMR structures are illustrated in Figure 14 [7]. GMR sensors can show changes in resistance of up to 20%.

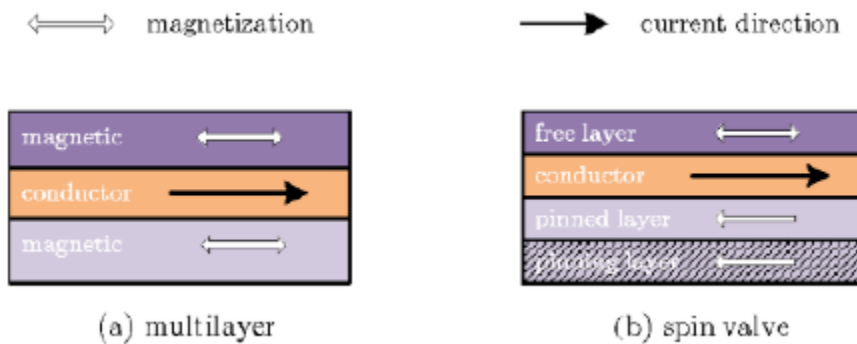


Figure 15: GMR structures

2.1.3 TMR Sensors

The most novel MR sensor technology is tunnel magnetoresistance. These sensors have a similar structure to GMR sensors, but the two ferromagnets are separated by an insulator or isolator instead of conductor. This insulator is very thin (usually around 1 nm) so that the electrons can tunnel from one ferromagnet to the other [6]. A common TMR structure can be seen in Figure 15 [7]. TMR sensors have shown changes in resistance greater than 100%. TMR sensors have shown much higher sensitivities when compared to GMR sensors, however as now they have a limited operating field range. They are a promising technology for future research.



Figure 16: TMR structure

2.1.4 Comparison of MR Sensors

Magnetoresistive sensors are a relatively new breed of sensing technology. GMR and TMR devices can be seen as expansions of the AMR effect, and they both exhibit much greater MR ratios than AMR sensors. Table 2 shows the evolution of MR sensors (data from TDK [25]).

Table 2: Evolution of MR Sensors

Sensor	Temperature Dependence (%/°C)	MR Ratio (%)
AMR	-0.29	~3
GMR	-0.23	~12
TMR	-0.13	>100

2.2 Applications of GMR Sensors

2.2.1 MRAM

The most notable large-scale application of GMR sensors to date is in the use of magnetoresistive random access memory (MRAM). The first MRAM device was developed in 1984 by Drs. Arthur Pohm and Jim Daughton while working at Honeywell [8]. The MRAM concept uses the natural hysteresis of magnetic materials to write data. Magnetic elements are arrayed so that those being written to receive a magnetic field above a certain threshold. The data is read depending on the differential resistance of the cell in the presence of a sense current. This current creates a magnetic field which opposes magnetization of the cell in one state, and is in the same direction in the other state [8]. An illustration of an early MRAM concept can be seen in Figure 16 [8].

MRAM was first introduced with a cobalt-permalloy alloy which exhibited an AMR of about 2%. The limitations of reading methods at the time meant that only 1/4 of this magnetoresistance, or 0.5%, could be sensed differentially. This allowed for read access times of about 250 ns [8]. The discovery of the GMR effect in 1988 allowed for higher magnetoresistance values and thus faster read times. At the time, GMR elements showed a

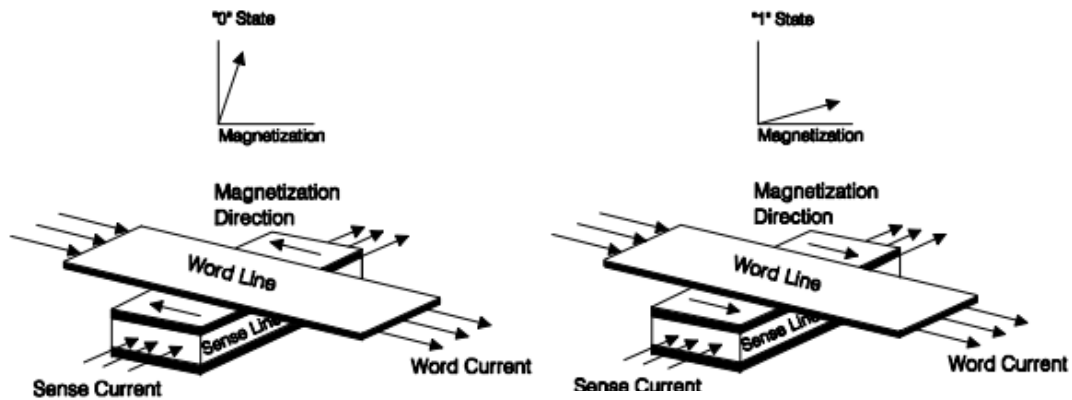


Figure 17: Early MRAM concept

magnetoresistance of approximately 6%. This improvement lead to read times under 50 ns [8]. The invention of the Psuedo-Spin Valve further improved MRAM, as now all of the 6% change in resistance could be reliably sensed. This made MRAM technologies more competitive with semiconductor memories at the time [8]. Modern MRAM cells use Spin Dependent Tunneling (SDT), which make use of tunnel magnetoresistance (TMR) values of up to 40% [8].

2.2.2 *Crankshaft Position Sensors*

Variable reluctance (VR) and Hall effect sensors are frequently used in crankshaft positioning systems. The gear tooth is made from a ferrous metal and thus the change in magnetic field can be sensed to provide a position output.

The output from VR sensors are proportional to the rate of change of the magnetic flux and not its magnitude. This can cause problems at low and high engine speeds. VR sensors are limited at low engine speeds as the voltage output drops to unusable levels. At high engine speeds, the effects of noise and electromagnetic interference (EMI) are more pronounced [9]. Hall effect sensors provide an output that is proportional to the magnitude of the magnetic field and therefore do not have the engine speed limitations seen in VR sensors [9]. However, most Hall effect sensors contain signal conditioning circuitry which greatly limits their performance over temperature.

Until recently, VR and Hall effect sensors were the two most obvious choices for crankshaft position detection. GMR sensors were tested for this application and compared to Hall effect sensors in [10]. The sensors were tested for use in wheel speed, crankshaft, and transmission rotational speed applications. The most important characteristic measured was the maximum air gaps for each application. The more air gap allowed results in a reduction in precision of mechanical parts, which can greatly reduce costs [10]. The performance of the sensors can be seen in Figure 17 [10]. It can be concluded that GMR sensors are a viable solution for crankshaft positioning detection. This can be attributed to their increased sensitivity and temperature stability when compared to Hall effect sensors.

Air gap	GMR-SV	GMR-ML	HALL	AMR
Wheel speed sensor (-40°C, 25°C, 170°C)	8 mm	7 mm	4.5 mm	/
Speed sensor: Crankshaft (-40°C, 25°C, 170°C)	7 mm	5.5 mm	3.5 mm	2.8 mm
Rotational speed sensor: Transmission (25°C)	9 mm	8 mm	5.1 mm	/

Figure 18: Maximum air gap attained using GMR (spin-valve and multilayer), Hall effect, and AMR sensors

2.3 GMR Sensors as Vibration Detectors

In [11], GMR sensors were used to detect perturbations in the earth's magnetic field due to vibrations of small ferromagnetic pieces. Two examples were setup to demonstrate this effect: one measured the rotating speed of a small drill bit set at different speeds and one measured the characteristic vibration of a 440-Hz tuning fork. Three sensors were used to measure vibrations in each axis (X, Y, Z). A generalized impedance converter (GIC) was used to reduce the power consumption of each sensor, and the outputs of each GMR

device were filtered and amplified by a factor of 1000, as can be seen in Figure 19 [11]. The high gain is needed as the magnetic field strength drops by a factor of r^3 . The filters are a combination of a high pass filter to remove the DC offset from each sensor and low pass filter to reduce the overall noise power of the system.

The spectra of the drill bits turning at given speeds differed heavily on whether the drill bit was well aligned or misaligned. For drill speeds of 4700 and 8500 rpm (78.3 and 141.6 Hz), the drill bit was well aligned and the only significant peak can be seen at the drill speed frequency, as expected. There are peaks at harmonic frequencies, but their small amplitudes indicate that the drill bits were well aligned. For a drill speed of 1800 rpm (30 Hz), results were taken with a well aligned drill bit and the with a drill bit that was intentionally strongly misaligned. The differences in spectra are very pronounced in the X-axis. The drill speed frequency is still present, but now the harmonic peaks have been enhanced and peaks occur at other, unrelated frequencies. These peaks are indicative of a fault condition in the system (in this system this fault was intentionally introduced). The spectrums of the different tests with drill bits can be seen in Figures 20 and 21 [11].

The detector also proved to be useful in sensing variations of the earth's magnetic field due to a vibrating tuning fork at 440 Hz. The small perturbations of the tuning fork still created peaks of approximately 50 dB and 30 dB above the noise floor in the X and Z axes. The spectrum of the tuning fork can be seen in Figure 22 [11].

A similar testing of GMR sensors was carried out in [12]. A machinery fault simulator with a rotating speed of 50 Hz was tested once with good bearing and once with faulty bearings. The harmonics of the rotating speed are enhanced in the system with faulty

bearings, as can be seen in Figure 23 [11]. A 440 Hz tuning fork was again tested in [12], and similar results to those seen in [11] can be seen in Figure 24 [12].

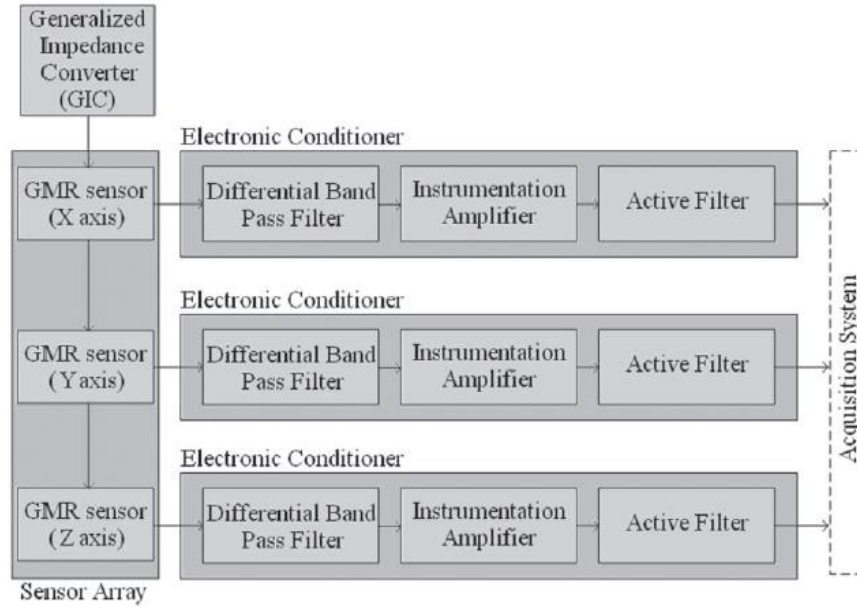


Figure 19: Block diagram of vibration detector discussed in [11]

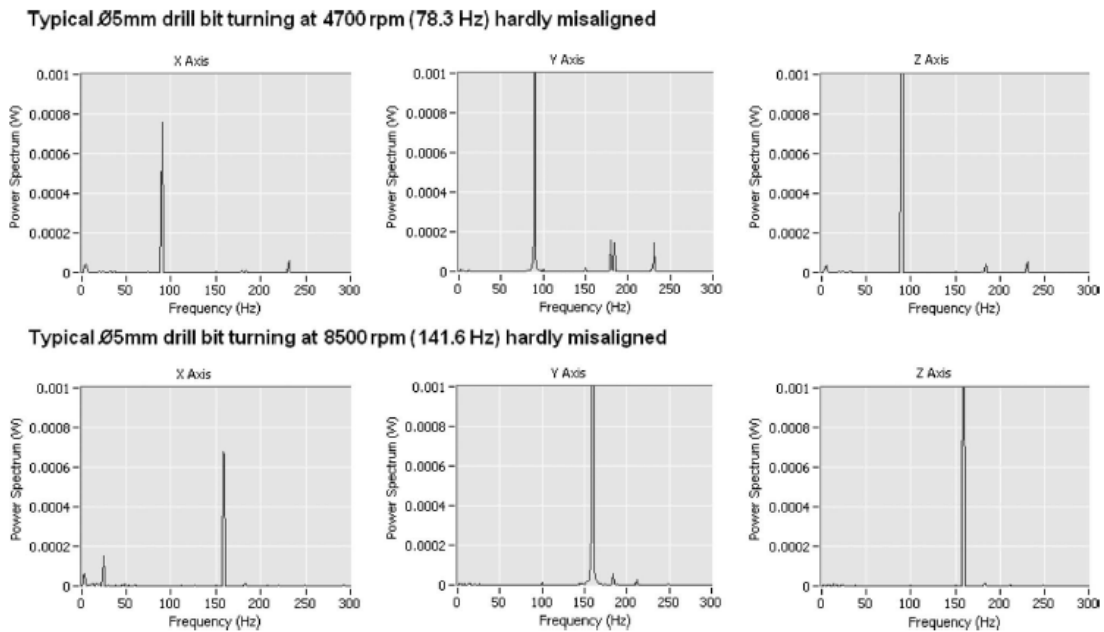


Figure 20: Signatures of well-aligned drill bits at 4700 and 8500 rpm. The only significant peaks occur at the frequency of the drill speed.

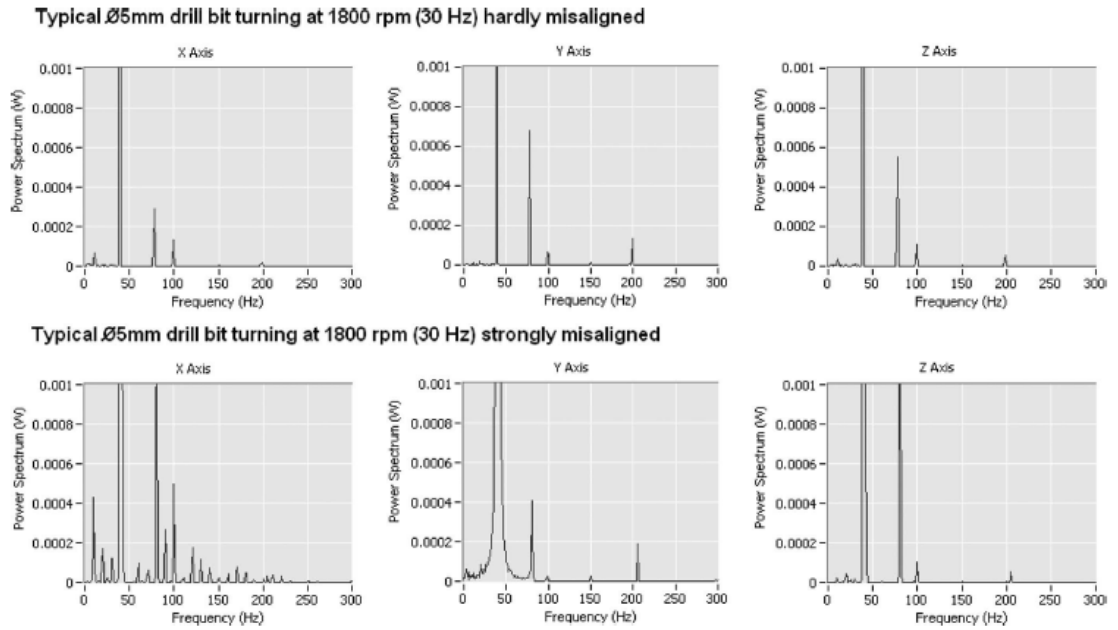


Figure 21: Signatures of a well-aligned and misaligned drill bit at 1800 rpm. Harmonic peaks have been enhanced and additional peaks are introduced.

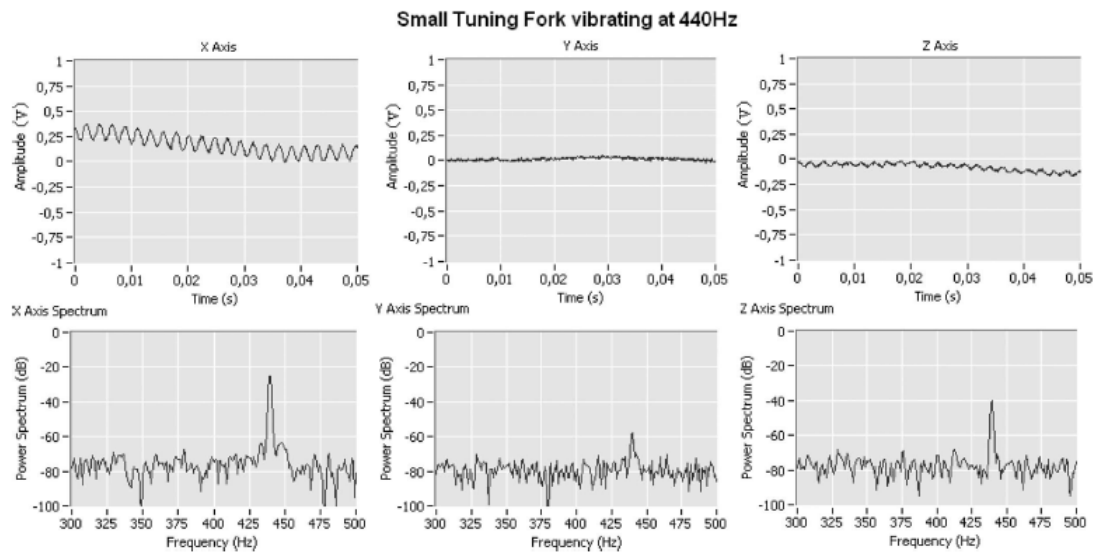


Figure 22: Signatures of the 440 Hz tuning fork in [11]

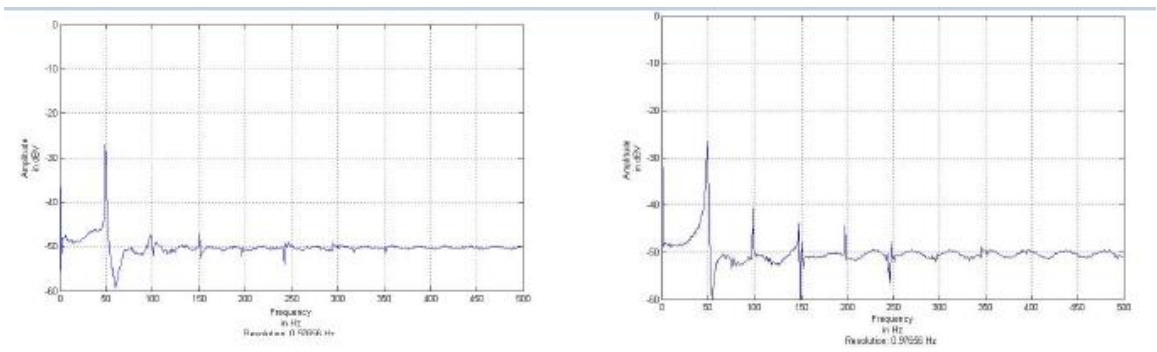


Figure 23: Signatures of machinery fault simulator with good bearings (left) and faulty bearings (right)

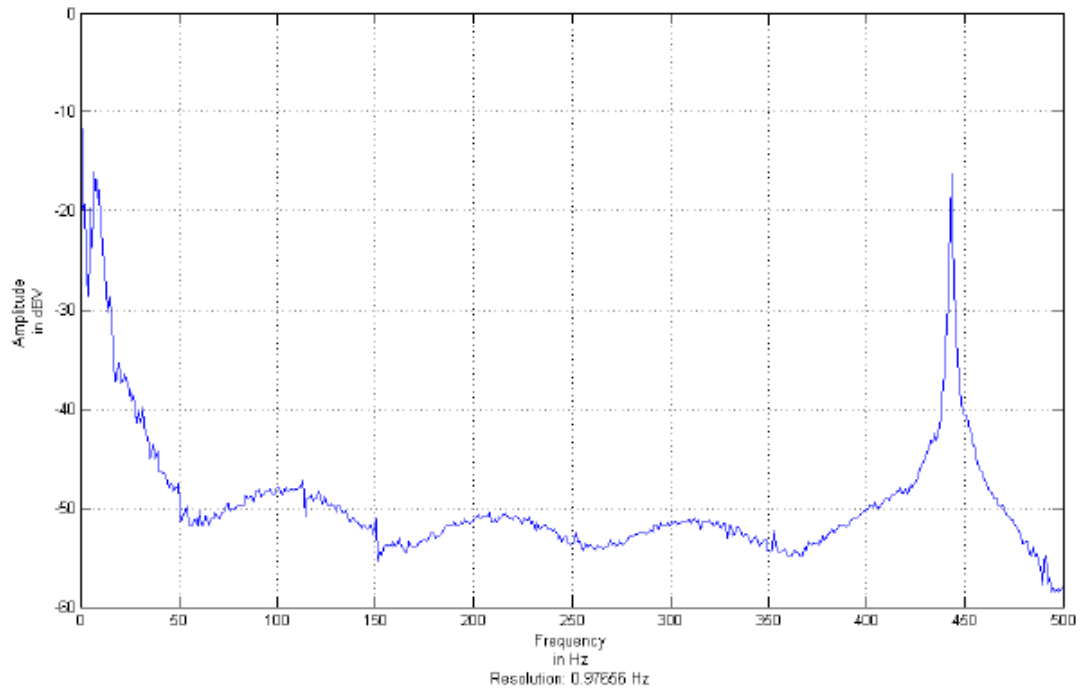


Figure 24: Signature of the 440 Hz tuning fork in [12]

CHAPTER 3. STRING VIBRATIONS

It can be seen from experiments in [11] and [12] that GMR sensors are a viable sensing mechanism for vibrations of ferromagnetic materials. The viability of GMR sensors was tested for use in sensing string vibrations in an electric guitar. Before going into the experimental results, the physics of string vibrations will be discussed as they are essential in understanding the empirical results.

3.1 The Wave Equation

Vibration in a string of length L , that is clamped at both ends, can most generally be described by the vertical displacement function $u(x, t)$, which satisfies the one-dimensional undamped wave equation [13]:

$$a^2 u_{xx} = u_{tt} \quad (3.1)$$

(where $a = \sqrt{\frac{\tau}{\rho}}$ and is the phase velocity, τ is the force on tension on the string, and ρ is the mass density of the string).

The equation is subjected to the boundary conditions:

$$u(0, t) = u(L, t) = 0 \quad (t > 0) \quad (3.2)$$

This simply shows that the two ends of the string are fixed and do not move [13]. There are also two initial conditions as the equation contains the second partial derivative with respect to time. They are:

$$u(x, 0) = f(x), u_t(x, 0) = g(x) \quad (3.3)$$

This reflects that both the initial vertical displacement, $f(x)$, and initial vertical velocity, $g(x)$, are only functions of x [13]. If $u(x, t) = X(x)T(t)$, the wave equation can be separated into two ODEs:

$$X'' + \lambda X = 0, X(0) = 0, X(L) = 0 \quad (3.4)$$

$$T'' + a^2 \lambda T = 0 \quad (3.5)$$

The solutions to the first eigenvalue problem are as follows:

$$\lambda = \frac{n^2 \pi^2}{L^2}, n = 1, 2, 3, \dots \quad (3.6)$$

$$X_n = \sin \frac{n\pi x}{L}, n = 1, 2, 3, \dots \quad (3.7)$$

After substituting the eigenvalues above into the second ODE, we have:

$$T'' + a^2 \frac{n^2 \pi^2}{L^2} T = 0 \quad (3.8)$$

The characteristic of the above has purely imaginary roots, namely:

$$r = \pm \frac{an\pi}{L} i \quad (3.9)$$

Which leads to the solution:

$$T_n(t) = A_n \cos\left(\frac{an\pi t}{L}\right) + B_n \sin\left(\frac{an\pi t}{L}\right), n = 1, 2, 3, \dots \quad (3.10)$$

After multiplying X and T and summing, the general solution is:

$$\boxed{u(x, t) = \sum_{n=1}^{\infty} \left(A_n \cos\left(\frac{an\pi t}{L}\right) + B_n \sin\left(\frac{an\pi t}{L}\right) \right) \sin\left(\frac{n\pi x}{L}\right)} \quad (3.11)$$

The Fourier coefficients are as follows:

$$A_n = \frac{2}{L} \int_0^L f(x) \sin\left(\frac{n\pi x}{L}\right) dx \quad (3.12)$$

$$B_n = \frac{2}{an\pi} \int_0^L g(x) \sin\left(\frac{n\pi x}{L}\right) dx \quad (3.13)$$

3.2 The Plucked String

It can be seen from (3.12) that if the initial vertical displacement $f(x) = 0$, then all $A_n = 0$. Similarly, from (3.13), if the initial vertical velocity $g(x) = 0$, then all $B_n = 0$. The plucked string is an example of the second case, $g(x) = 0$ and thus all $B_n = 0$. Therefore, for a plucked string, (3.11) can be simplified to [13]:

$$u(x, t) = \sum_{n=1}^{\infty} A_n \sin\left(\frac{n\pi x}{L}\right) \cos\left(\frac{an\pi t}{L}\right) \quad (3.14)$$

Solving for A_n involves a fairly complex integration by parts. The solution comes to be [14-16]:

$$A_n = \frac{2hL^2}{\pi^2 n^2 d(L-d)} \sin\left(\frac{n\pi d}{L}\right) \quad (3.15)$$

(where h is the vertical amplitude of the pluck and d is the horizontal plucking position).

The vertical displacement for a plucked string becomes:

$$u(x, t) = \sum_{n=1}^{\infty} \frac{2hL^2}{\pi^2 n^2 d(L-d)} \sin\left(\frac{n\pi d}{L}\right) \sin\left(\frac{n\pi x}{L}\right) \cos\left(\frac{an\pi t}{L}\right) \quad (3.16)$$

3.2.1 Harmonic Amplitudes

It can be concluded from (3.15) that the relative amplitude of the n th harmonic to the fundamental is [15]:

$$\frac{A_n}{A_1} = \frac{\sin\left(\frac{n\pi d}{L}\right)}{n^2 \sin\left(\frac{\pi d}{L}\right)} \quad (3.17)$$

It must be noted, however, that a traditional inductive pickup senses the velocity of the vibrating string rather than its position. In order to calculate the Fourier coefficients of the velocity of the string, a time derivative of the ideal string model must be taken [16]. The relative amplitude of the n th harmonic to the fundamental of the velocity of the string becomes [16]:

$$\frac{V_n}{V_1} = \frac{\sin\left(\frac{n\pi d}{L}\right)}{n \sin\left(\frac{\pi d}{L}\right)} \quad (3.18)$$

(where V is used instead of A to imply that these are the coefficients of *velocity* rather than displacement).

Equation (3.18) differs from (3.17) by a factor of n in the denominator. This implies that, when sensing the velocity of the string, the higher order harmonics are less suppressed than when sensing the position of the string.

Equations (3.18) and (3.17) only describe the spatial dependence of the plucking point of the string, and do not include the dependence of the sensing position along the string. The dependence of the sensing location is described by the second sine function in (3.16). The displacement function can be rewritten to include all spatial dependences in A as follows:

$$u(x, t) = \sum_{n=1}^{\infty} A'_n \cos\left(\frac{an\pi t}{L}\right) \quad (3.19)$$

$$A'_n = \frac{2hL^2}{\pi^2 n^2 d(L-d)} \sin\left(\frac{n\pi d}{L}\right) \sin\left(\frac{n\pi x}{L}\right) \quad (3.20)$$

The ratio of the n th harmonic to the fundamental of A' is:

$$\frac{A'_n}{A'_1} = \frac{\sin\left(\frac{n\pi d}{L}\right) \sin\left(\frac{n\pi x}{L}\right)}{n^2 \sin\left(\frac{\pi d}{L}\right) \sin\left(\frac{\pi x}{L}\right)} \quad (3.21)$$

and similarly, for V' :

$$\frac{V'_n}{V'_1} = \frac{\sin\left(\frac{n\pi d}{L}\right) \sin\left(\frac{n\pi x}{L}\right)}{n \sin\left(\frac{\pi d}{L}\right) \sin\left(\frac{\pi x}{L}\right)} \quad (3.22)$$

Equations (3.21) and (3.22) show that for a string plucked at a distance d , the spectrum sensed at a distance x will have nulls at multiples of $n = L / d$ and multiples of $n = L / x$. This can be seen in Figure 25 [16].

3.2.1.1 Plucking and Pickup Width Effects

In addition to the plucking and pickup locations, the widths of the plucking mechanism and pickup also affect the harmonic spectrum [16-18]. The previous equations

assume a plucking mechanism of infinitesimally small width sensed at a single point. When taking into account a plucking mechanism of finite width δ sensed with a pickup of width w , a 6 dB/octave roll-off occurs above $n = 2L / (\pi\delta)$ and $n = 2L / (\pi w)$ [16-18]. Combining the two width effects, the spectrum is limited to $n < \min(\frac{2L}{\delta}, \frac{2L}{w})$ [16-18].

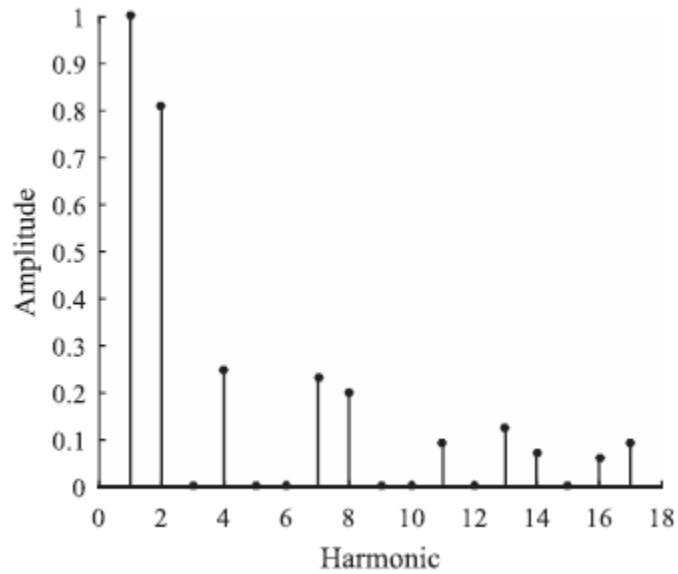


Figure 25: Ideal string model (velocity) of a string plucked at 1/3 of its length with the pickup placed at 1/5 of its length

CHAPTER 4. GMR SENSORS AS ELECTRIC GUITAR PICKUPS

GMR sensors were tested as with a prototype electric guitar in [19]. The sensors were compared to the classic inductive pickup in their response to external magnetic fields. The GMR pickup was much less sensitive to external fields (~ 200 times at 50 Hz and ~ 1000 times at 5 kHz). These results are due to the fact that the GMR elements have a much smaller sensor area when compared to inductive pickups ($\sim 0.5 \text{ mm}^2$ compared to $\sim 600 \text{ mm}^2$) [19]. The results under external fields can be seen in Figures 26 and 27 [19].

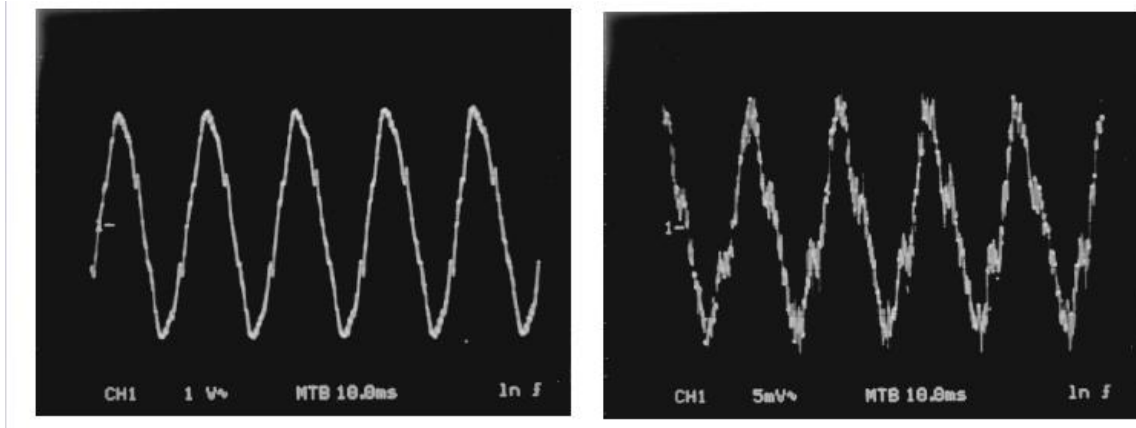


Figure 26: Inductive pickup (left) and GMR (right) response to 50 Hz mains hum

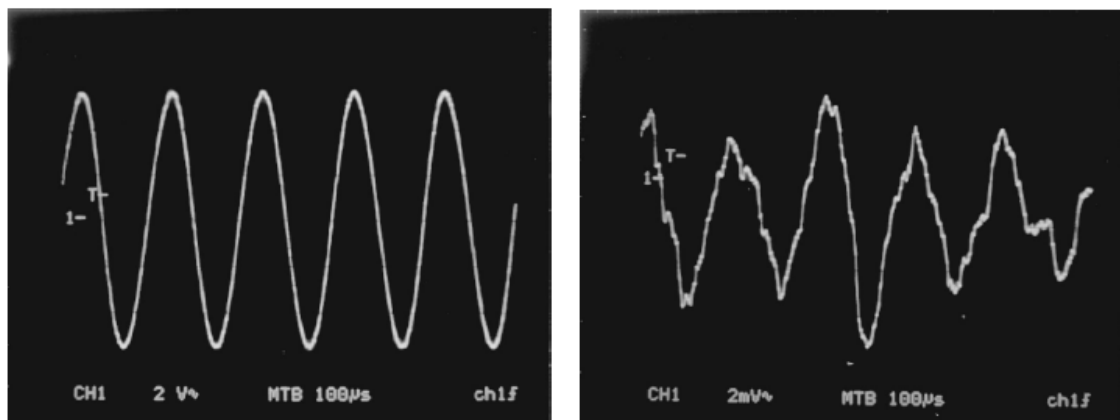


Figure 27: Inductive pickup (left) and GMR (right) response to 5 kHz external field

In [20], GMR sensors were compared to both inductive pickups and Hall effect sensors. The sensors were tested for sensitivity and signal-to-noise ratio (SNR) using the guitar's G string (196 Hz fundamental). The results show that the GMR greatly outperforms the Hall effect pickup in SNR and is comparable to the inductive pickup. The GMR sensor showed a lower sensitivity to the Hall effect sensor in this experiment, which is probably due to the fact that the sensor was operated with the minimum supply voltage (thus reducing the bridge output). The results can be seen in Figure 28 [20].

	GMR (AA005)	Inductive Epiphone 650R & 720T Humbucker	Hall (A1324)	Unit
Gain	1000	1	50	V/V
Output Signal Size	2.84	0.6	0.5	V _{pp}
Output Noise	1.0528	0.32962	10.266	mV _{rms}
Scope Noise	0.21517	0.21517	0.21517	mV _{rms}
Effective Noise	0.83763	0.11445	10.05083	mV _{rms}
SNR	61.57311	65.3585	24.90315	dB

Figure 28: Signal strength and noise comparison from [20]

CHAPTER 5. EXPERIMENTAL RESULTS

A GMR sensor was tested for detecting string vibrations, namely the low E string (82.41 Hz fundamental). The main purpose of the tests was to compare the harmonic spectrum produced by the GMR sensor to the spectrum produced by the inductive pickup equipped on the guitar itself.

5.1 Sensor Characteristics

The AA005 sensor from NVE was used for this experiment. It is a uses a standard multilayer structure and the elements are in a half-bridge configuration. The multilayer structure results in a resistance change of 12-16% [21]. Four GMR elements are placed in a bridge, with two of them being magnetically shielded. The two unshielded elements change resistance with an applied magnetic field and imbalance the bridge. This imbalance results in a voltage difference across the bridge. The resultant output voltage is [22]:

$$V_{out} = V_s \frac{\Delta R/R}{2+\Delta R/R} \quad (5.1)$$

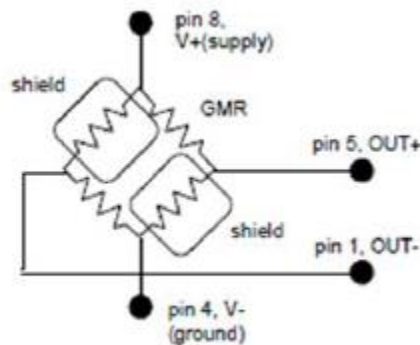


Figure 29: Half-bridge sensor setup (Source: NVE Corporation)

The AA005 sensor was chosen as it has sufficient sensitivity for the application and also a wide linear range. The characteristics of the AA005 sensor can be seen in Figure 29 [23]. The sensor was operated off a 15 V supply, resulting in a sensitivity of ~8.25 mV/Oe (1 Oe = 1 Gauss).

Available Part	Linear Range (lOe)		Saturation (lOe)	Sensitivity (mV/V-Oe)		Max. Non-linearity (% Uni.)	Max. Hysteresis (% Uni.)	Max. Operating Temp.	Typ. Resistance	Package
	Min.	Max.		Min.	Max.					
AA005-02	10	70	100	0.45	0.65	2%	4%	125°C	5 kΩ	SOIC8

Figure 30: AA-005 Sensor Characteristics (Source: NVE Corporation)

5.2 Circuit Design and Testing Setup

A simple bridge amplifier circuit was designed to obtain a usable signal from the GMR sensor element. The circuit design was based off recommendations from the manufacturer, NVE [23]. The circuit consists of the bridge sensor, a differential high-pass filter, an instrumentation amplifier, and an output low-pass filter. The circuit diagram can be seen in Figure 30. The differential high-pass filter removes the DC offset from the GMR sensor (created by the permanent magnet on the guitar). This allows for more headroom to amplify the time-varying output of the sensor. The INA128 instrumentation amplifier from Texas Instruments was chosen as it has a very good common-mode rejection ratio, especially at high gain. The gain was set at 5000 ($R_G = 10 \Omega$). A low-pass filter with cutoff

of 3 kHz was added before the output to reduce the overall noise-power of the system [24]. The cutoff was chosen to leave significant harmonics unaffected.

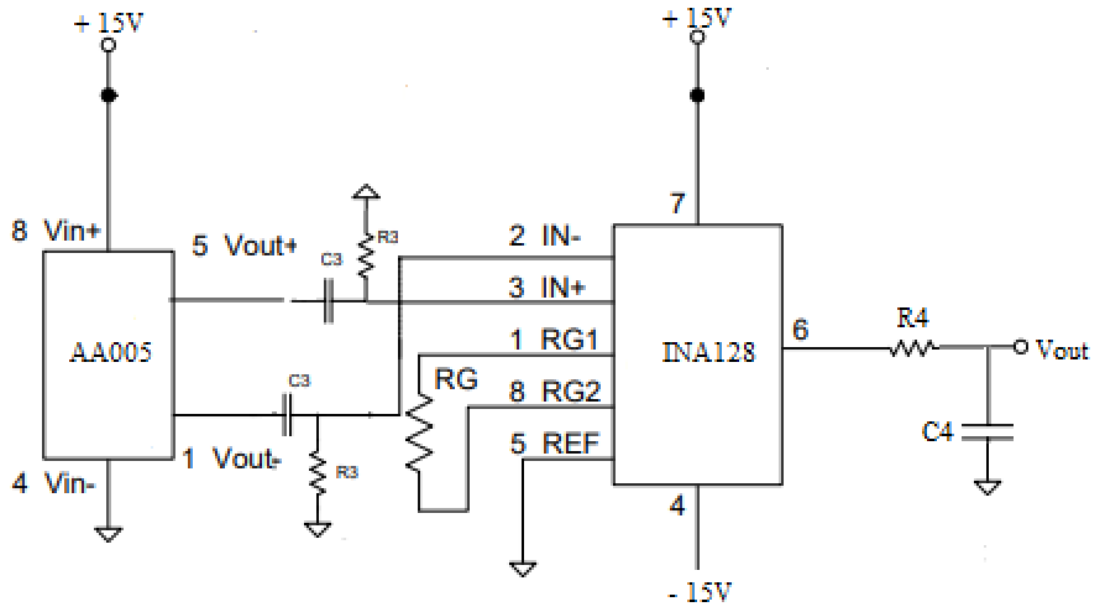


Figure 31: Bridge amplifier used with AA005 sensor ($R_3 = 10 \text{ M}\Omega$, $R_4 = 510$, $C_3 = C_4 = 0.1 \mu\text{F}$)

The testing setup for the GMR sensor can be seen in Figure 32. The sensor was placed $\sim 9.5 \text{ mm}$ below the string. The signal from the inductive sensor was taken from the stereo jack on the guitar. It was amplified by a factor of 50 to make the amplitude comparable to the GMR output. Tone controls were turned off to give a true representation of the pickup output. The scale length of the string was 63.5 cm.

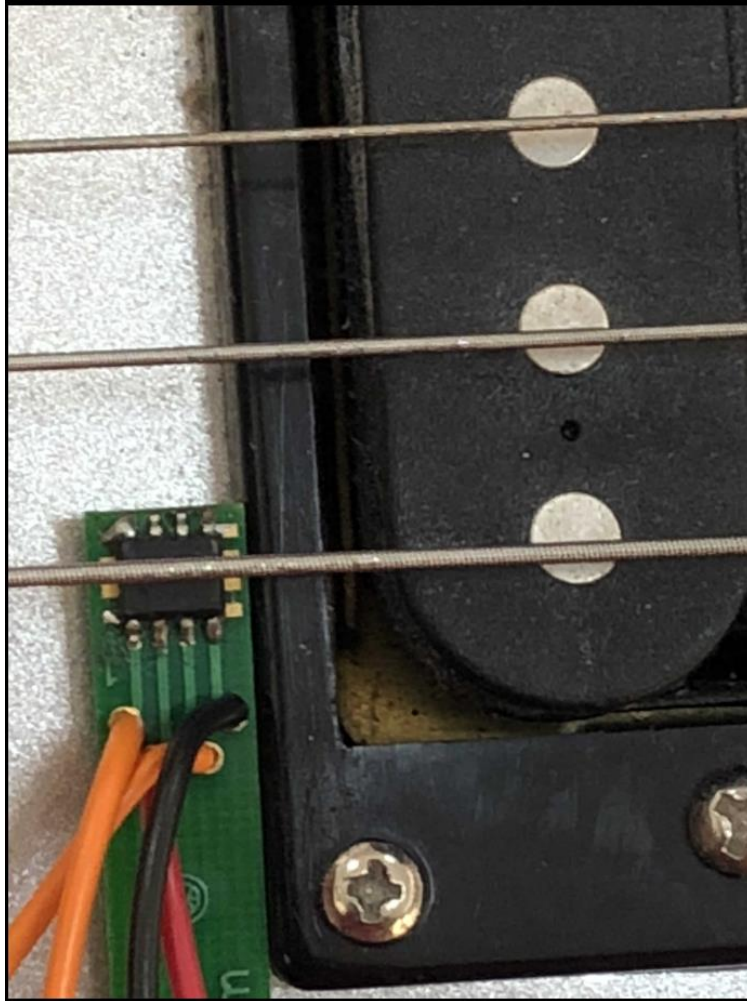


Figure 32: GMR sensor (left) and inductive pickup (right)

5.3 Results

The GMR sensor and inductive pickup were tested simultaneously (e.g. results were taken for both with the same string pluck). The plucking mechanism had a width of ~ 0.7 mm to avoid any adverse effects. The low E string was plucked at $1/2$, $1/3$, and $1/4$ of its length and the GMR sensor was placed at 12.7 cm (near the neck pickup) and 7.6 cm (near the bridge pickup) from the bridge of the guitar. This corresponds to $1/5$ and $\sim 1/8$ of the scale length. The inductive pickup on the guitar does not sense the velocity at a single point,

but rather at the neck *and* the bridge. It follows that, for a mixed pickup, (3.22) is altered to [16,18]:

$$\frac{V'_n}{V'_1} = \frac{\sin\left(\frac{n\pi d}{L}\right)\left[\sin\left(\frac{n\pi x_1}{L}\right) + \sin\left(\frac{n\pi x_2}{L}\right)\right]}{n \sin\left(\frac{\pi d}{L}\right)\left[\sin\left(\frac{\pi x_1}{L}\right) + \sin\left(\frac{\pi x_2}{L}\right)\right]} \quad (5.2)$$

where x_1 and x_2 are the centers of each humbucker pickup (14.6 cm and 4.45 cm respectively).

Time domain data for both the GMR and inductive pickup was taken using an oscilloscope. Data was taken for 1 second with a sampling rate of 62.5 kHz. The Fourier transform was applied using MATLAB, and a Kaiser windowing function with $\alpha = 16$ was applied.

The harmonic spectra produced by both the GMR sensor and inductive pickup are presented and compared to the theoretical values from (3.21) and (5.2).

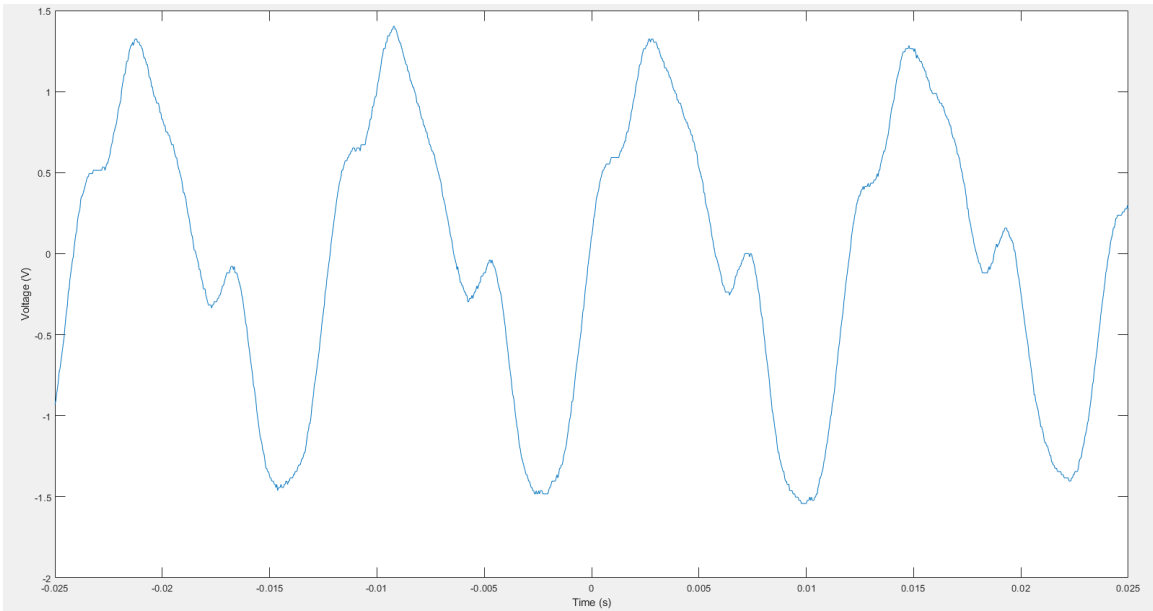


Figure 33: Time domain plot of GMR output

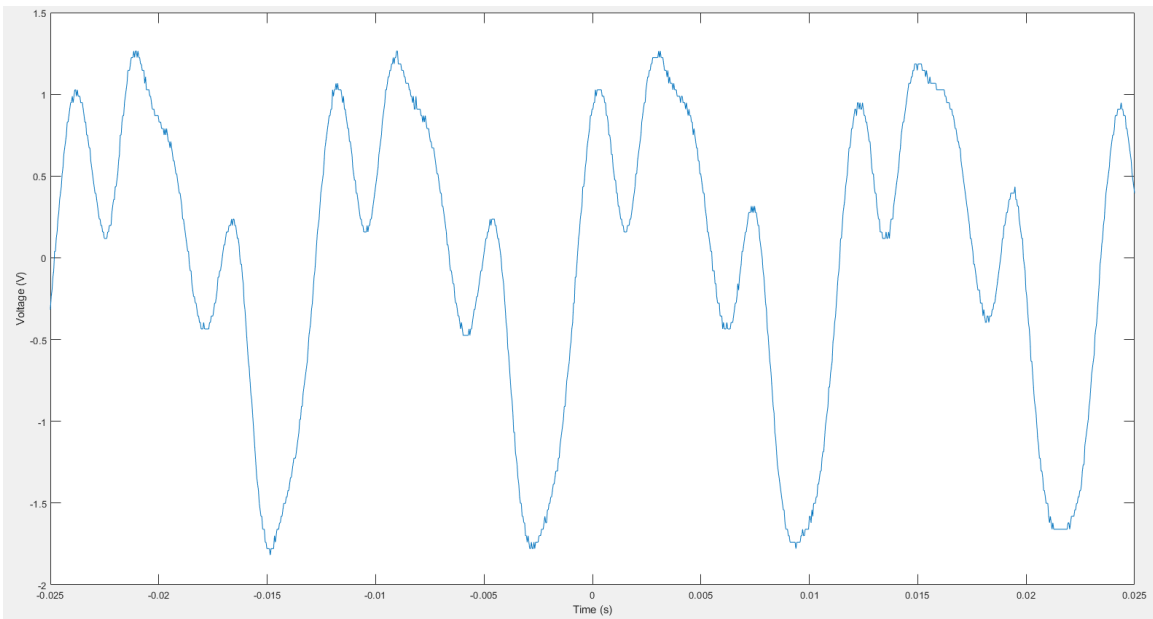


Figure 34: Time domain plot of inductive pickup output

5.3.1 GMR Sensor Placed Near Neck Pickup

5.3.1.1 String Plucked at 1/4 Length

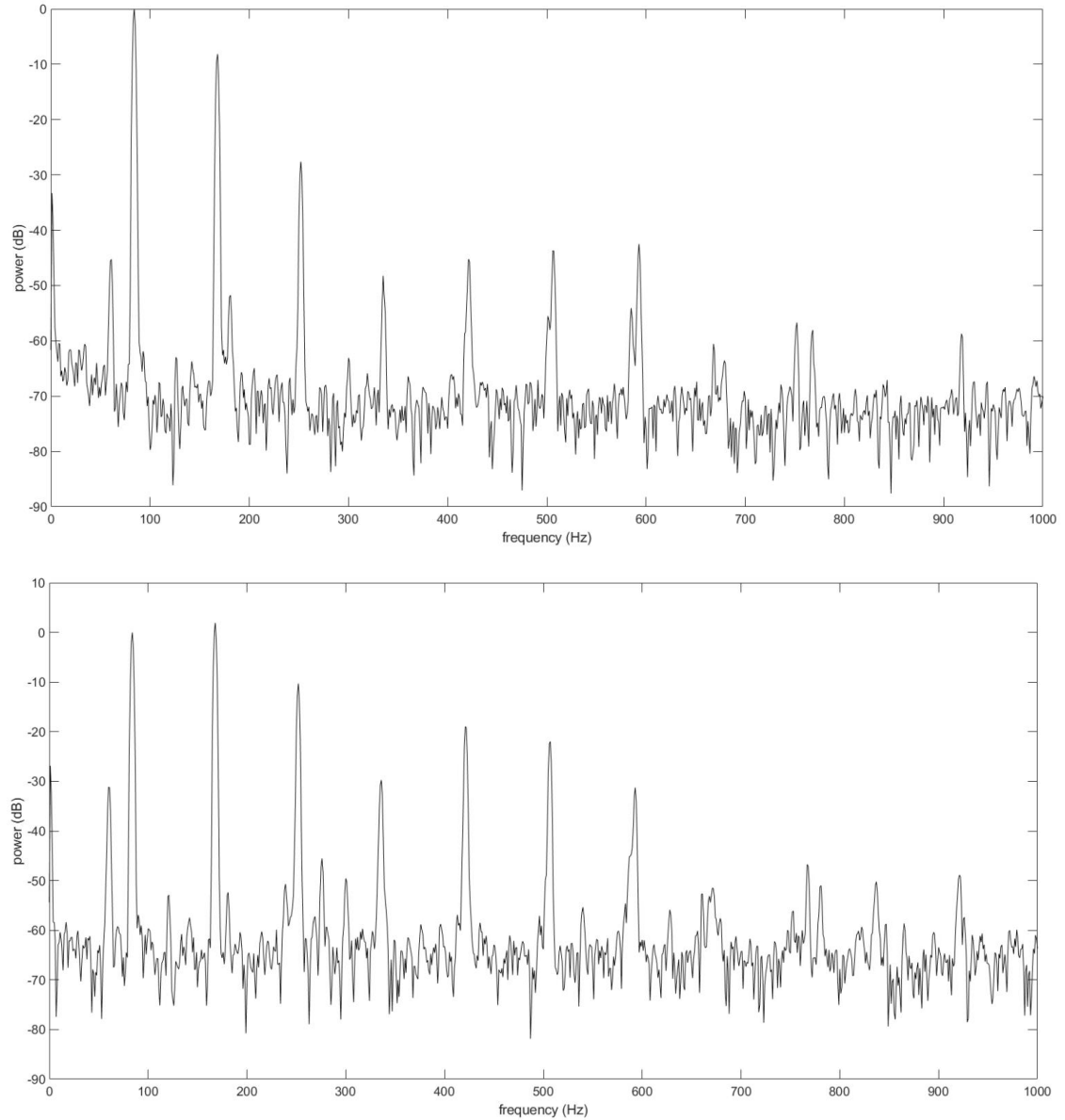


Figure 35: Spectrum of GMR (top) and inductive (bottom) pickup for a string plucked at 1/4 length with the GMR element placed at 1/5 length

Table 3: GMR Amplitudes for String Plucked at 1/4 Length and Sensor at 1/5 Length

Harmonic	Measured Amplitude Relative to Fundamental	Theoretical Value from (3.21)	Absolute Error
2	0.391832	0.572061	0.180229
3	0.041639	0.179782	0.138143
4	0.003873	0	0.003873
5	0.005464	0	0.005464
6	0.006554	0.039284	0.032730
7	0.00749	0.033021	0.025531
8	0.000939	0	0.000939

Table 4: Inductive Pickup Amplitudes for String Plucked at 1/4 Length

Harmonic	Measured Amplitude Relative to Fundamental	Theoretical Value from (5.2)	Absolute Error
2	1.247958	1.140030	0.107928
3	0.305844	0.545788	0.239944
4	0.032584	0	0.032584
5	0.11272	0.099383	0.013337
6	0.079708	0.010401	0.069307
7	0.027321	0.009523	0.017798
8	0.002633	0	0.002633

5.3.1.2 String Plucked a 1/3 Length

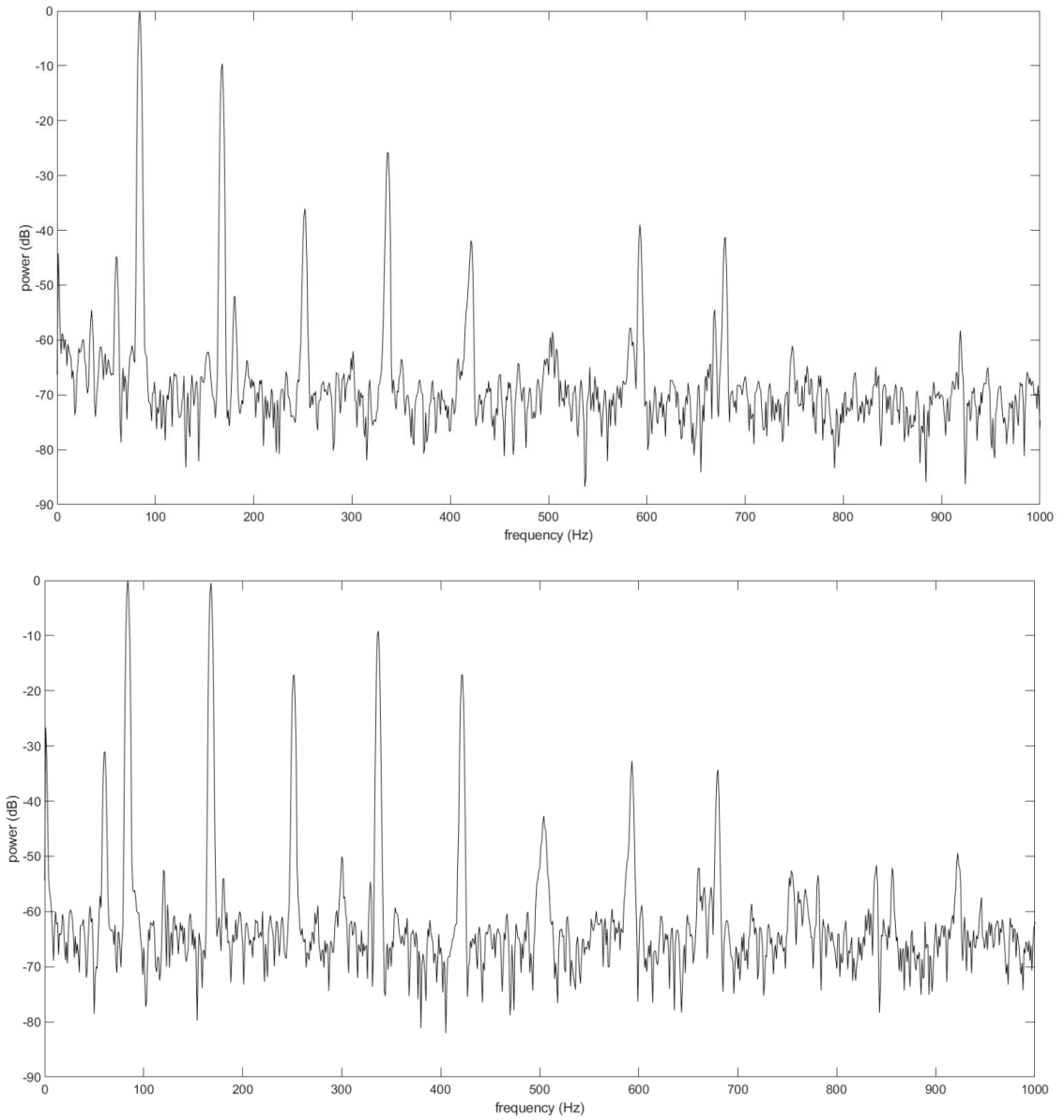


Figure 36: Spectrum of GMR (top) and inductive (bottom) pickup for a string plucked at 1/3 length with the GMR element placed at 1/5 length

Table 5: GMR Amplitudes for String Plucked at 1/3 Length and Sensor at 1/5 Length

Harmonic	Measured Amplitude Relative to Fundamental	Theoretical Value from (3.21)	Absolute Error
2	0.331551	0.404508	0.072957
3	0.015776	0	0.015776
4	0.051464	0.0625	0.011036
5	0.008063	0	0.008063
6	0.001184	0	0.001184
7	0.011194	0.033021	0.021827
8	0.00864	0.025282	0.016642

Table 6: Inductive Pickup Amplitudes for String Plucked at 1/3 Length

Harmonic	Measured Amplitude Relative to Fundamental	Theoretical Value from (5.2)	Absolute Error
2	0.950167	0.806121	0.144046
3	0.138995	0	0.138995
4	0.347056	0.289726	0.057330
5	0.138995	0.099383	0.039612
6	0.007337	0	0.007337
7	0.023147	0.009523	0.013624
8	0.019231	0.071142	0.051911

5.3.1.3 String Plucked at 1/2 Length

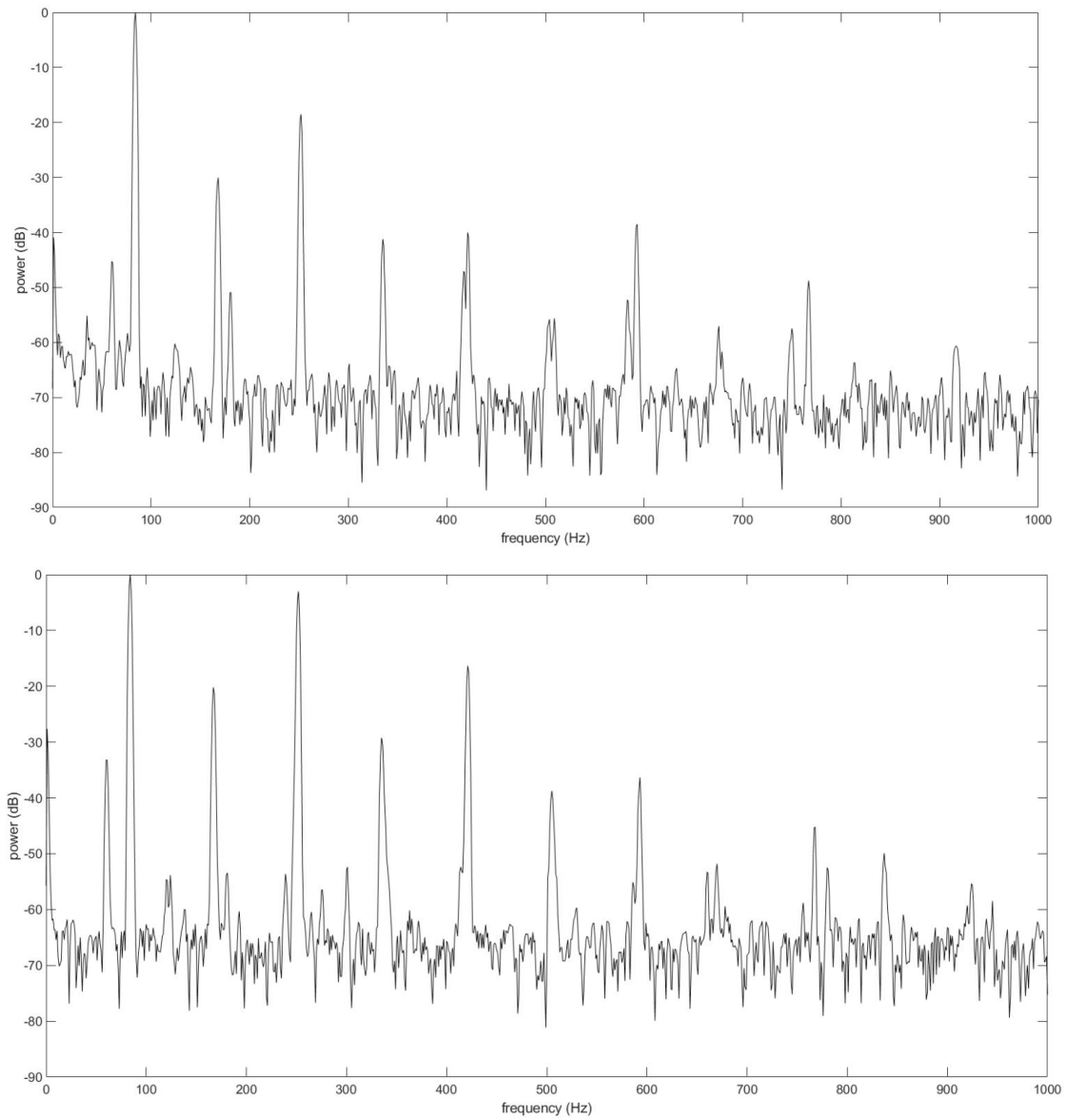


Figure 37: Spectrum of GMR (top) and inductive (bottom) pickup for a string plucked at 1/2 length with the GMR element placed at 1/5 length

Table 7: GMR Amplitudes for String Plucked at 1/2 Length and Sensor at 1/5 Length

Harmonic	Measured Amplitude Relative to Fundamental	Theoretical Value from (3.21)	Absolute Error
2	0.031477	0	0.031477
3	0.11885	0.179782	0.060932
4	0.00871	0	0.008710
5	0.009988	0	0.009988
6	0.001624	0	0.001624
7	0.011899	0.033021	0.021122
8	0.001408	0	0.001408

Table 8: Inductive Pickup Amplitudes for String Plucked at 1/2 Length

Harmonic	Measured Amplitude Relative to Fundamental	Theoretical Value from (5.2)	Absolute Error
2	0.097724	0	0.097724
3	0.707050	0.545788	0.161262
4	0.034594	0	0.034594
5	0.15223	0.099383	0.052847
6	0.011535	0	0.011535
7	0.015258	0.009523	0.005735
8	0.002570	0	0.002570

5.3.2 GMR Sensor Placed Near Bridge Pickup

5.3.2.1 String Plucked at 1/4 Length

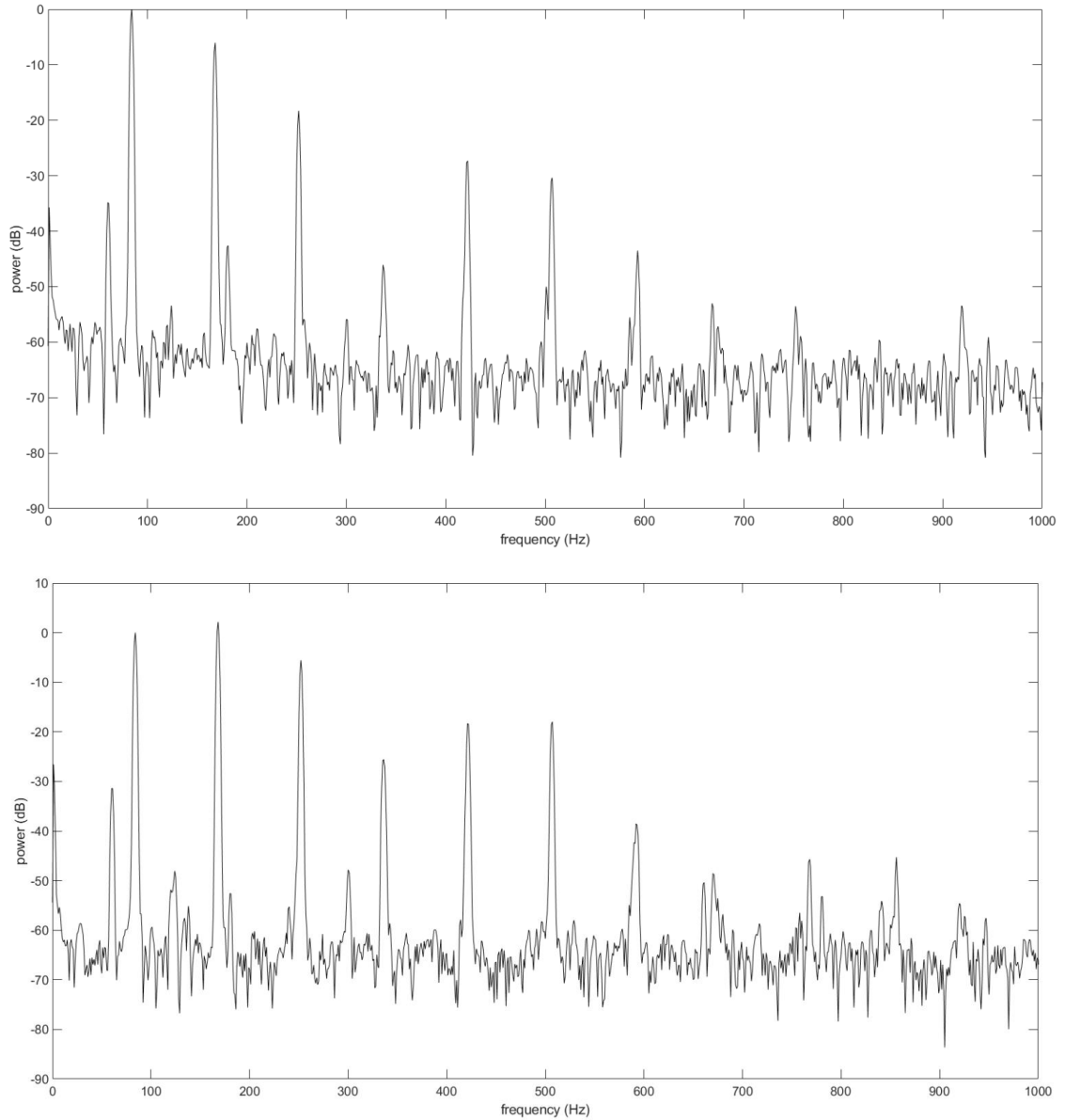


Figure 38: Spectrum of GMR (top) and inductive (bottom) pickup for a string plucked at 1/4 length with the GMR element placed at $\sim 1/8$ length

Table 9: GMR Amplitudes for String Plucked at 1/4 Length and Sensor at ~1/8 Length

Harmonic	Measured Amplitude Relative to Fundamental	Theoretical Value from (3.21)	Absolute Error
2	0.498024	0.657451	0.159427
3	0.121759	0.273104	0.151345
4	0.004966	0	0.004966
5	0.042954	0.103340	0.060386
6	0.030269	0.082224	0.051955
7	0.006683	0.026708	0.020025
8	0.002234	0	0.002234

Table 10: Inductive Pickup Amplitudes for String Plucked at 1/4 Length

Harmonic	Measured Amplitude Relative to Fundamental	Theoretical Value from (5.2)	Absolute Error
2	1.282478	1.209891	0.072587
3	0.526441	0.647161	0.120720
4	0.052602	0	0.052602
5	0.121479	0.198985	0.077506
6	0.126328	0.045056	0.081272
7	0.011442	0.070136	0.058694
8	0.003728	0	0.003728

5.3.2.2 String Plucked at 1/3 Length

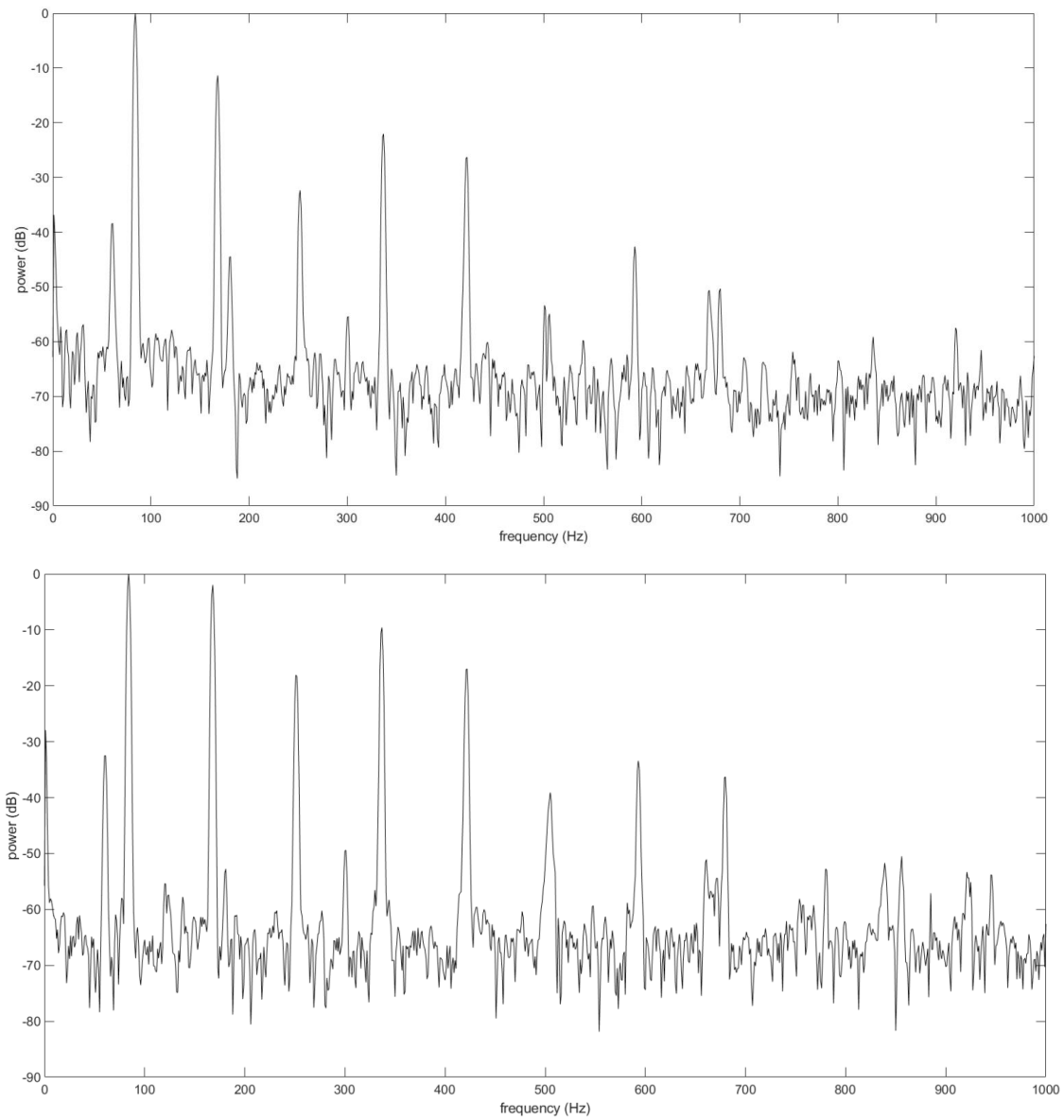


Figure 39: Spectrum of GMR (top) and inductive (bottom) pickup for a string plucked at 1/3 length with the GMR element placed at $\sim 1/8$ length

Table 11: GMR Amplitudes for String Plucked at 1/3 Length and Sensor at ~1/8 Length

Harmonic	Measured Amplitude Relative to Fundamental	Theoretical Value from (3.21)	Absolute Error
2	0.269774	0.464888	0.195114
3	0.024071	0	0.024071
4	0.078886	0.169444	0.090558
5	0.048417	0.103340	0.054923
6	0.002145	0	0.002145
7	0.007396	0.026708	0.019312
8	0.002948	0.005320	0.002372

Table 12: Inductive Pickup Amplitudes for String Plucked at 1/3 Length

Harmonic	Measured Amplitude Relative to Fundamental	Theoretical Value from (5.2)	Absolute Error
2	0.795976	0.855522	0.059546
3	0.124451	0	0.124451
4	0.331093	0.414739	0.083646
5	0.141416	0.198985	0.057569
6	0.011092	0	0.011092
7	0.021281	0.070136	0.048855
8	0.015293	0.107976	0.092683

5.3.2.3 String Plucked at 1/2 Length

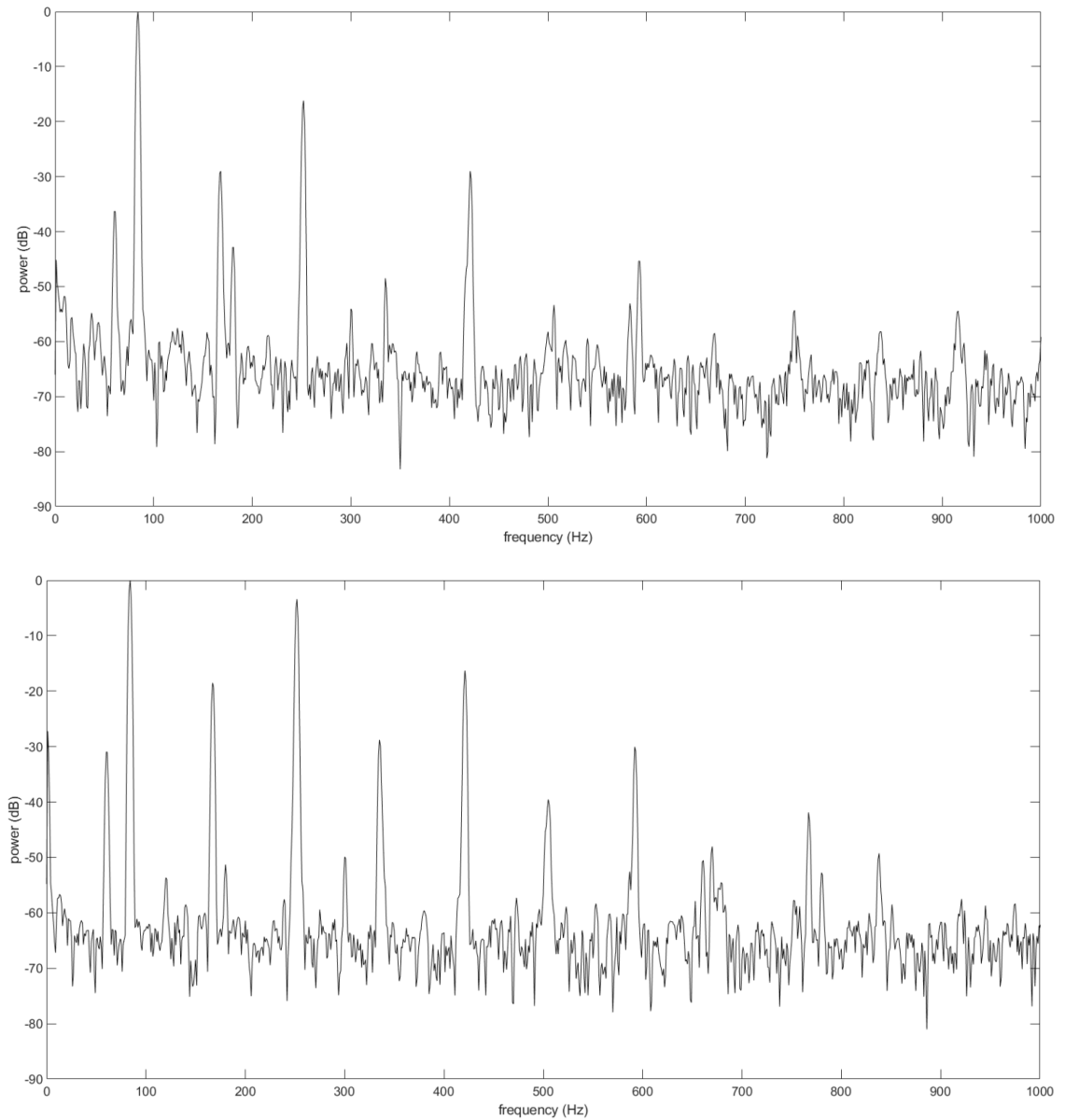


Figure 40: Spectrum of GMR (top) and inductive (bottom) pickup for a string plucked at 1/2 length with the GMR element placed at $\sim 1/8$ length

Table 13: GMR Amplitudes for String Plucked at 1/2 Length and Sensor at ~1/8 Length

Harmonic	Measured Amplitude Relative to Fundamental	Theoretical Value from (3.21)	Absolute Error
2	0.035441	0	0.035441
3	0.155239	0.273104	0.117865
4	0.003767	0	0.003767
5	0.035522	0.103340	0.067818
6	0.002145	0	0.002145
7	0.005389	0.026708	0.021319
8	0.00119	0	0.001190

Table 14: Inductive Pickup Amplitudes for String Plucked at 1/2 Length

Harmonic	Measured Amplitude Relative to Fundamental	Theoretical Value from (5.2)	Absolute Error
2	0.118713	0	0.118713
3	0.675461	0.647161	0.028300
4	0.03635	0	0.036350
5	0.153285	0.198985	0.045700
6	0.010532	0	0.010532
7	0.031405	0.070136	0.038731
8	0.003967	0	0.003967

5.3.3 Conclusions

The results proved inconsistent for both the GMR sensor and inductive pickup. The GMR sensor proved very adept in sensing nulls in the spectrum related to plucking and pickup positions, as relative amplitudes corresponding to these harmonics were closer to zero than corresponding amplitudes from the inductive pickup. Some results from both the GMR and inductive pickup correlated to the theoretical values, however, many relative amplitudes did not match the theoretical values.

A main source of error for the GMR sensor was its sensitivity. As n increases, the vertical displacement of the string decreases. In addition to this, the magnetic field sensed decreases with a factor of $1/r^3$. The output of the GMR sensor was less than the expected value from (3.21) in every case. It can also be seen that the error increases with n . This indicates that the GMR sensor did not have adequate sensitivity to sense smaller displacement changes. For higher order harmonics, the amplitudes fall close to the noise floor and thus the error increases. For future research, TMR sensors should be considered as they have sensitivities of more than 5 times that of GMR sensors.

For the inductive pickup, the main source of error is the individual windings and magnet strengths of the neck and bridge pickups. In many guitars, one pickup is equipped with a stronger magnet and more windings to increase the voltage sensed at that point. This is commonly done on the bridge pickup as the displacement of the string is substantially less at the bridge than at the neck. These imbalances cause the spectrum to deviate from its expected values. For instance, if the bridge pickup is wound with twice as much wire than the neck pickup, (5.2) must include a coefficient of 2 for the sine functions correlating to

that pickup. As these parameters were not precisely known for this experiment, the results can be quite inconsistent. For future research, a string apparatus and pickups should be designed rather than using an existing guitar. This will lead to more predictable results.

An additional source of error for both the GMR and inductive pickup is the initial plucking of the string. For each pickup and plucking position, the string was plucked down across the string (mimicking the strumming of a guitar string). This results in an elliptical rather than vertical string vibration. The variation in magnetic field strength is therefore more complex due to the introduction of horizontal vibrations. In order to keep consistent with predictions in (3.21) and (5.2), the string would need to be excited in a manner that restricts horizontal motion. It is difficult, however, to practically isolate vertical and horizontal string motion without interfering with the natural vibration of the string. A comparison of the spectra from a pluck down across the string versus a string given a purely vertical initial displacement (e.g. with a thin tweezer) is advised for future research.

CHAPTER 6. CONCLUSION

Detecting vibrations is a necessity in many industries. In many cases, vibrations are an indication of a fault condition in a machine or system. The spectrum produced by GMR sensors proved to be useful in detecting faults in drill bits and other machines. Their performance over temperature is significantly better than Hall effect devices which is very important in many industries.

The GMR sensors also proved to be viable in detecting string vibrations. The flat frequency response can be utilized in predicting plucking and pickup locations of guitar players, as the spectrum produced is not affected by the sensor itself which is the case with inductive pickups. It should be noted that the spectrum produced by one string is much easier to predict than when multiple strings are vibrating, as the interference produced by each string will influence the spectrum of sensors intended for adjacent strings.

For future research, it is recommended that a customized string apparatus and pickups are used instead of using an existing guitar. Guitar manufacturers differ greatly in how the pickups are designed and how the signal is routed to the amplifier. Control of these two elements will lead to more predictable results. TMR sensors are also advised for use in future research. These sensors have considerably higher sensitivities than GMR sensors and can provide much better resolution for higher order harmonics.

REFERENCES

- [1] A. G. Piersol, T. L. Paez, and C. M. Harris, *Harris shock and vibration handbook*, 5th ed. New York: McGraw-Hill, 2010.
- [2] J. S. Wilson, *Sensor technology handbook*. Burlington: Elsevier, 2011.
- [3] J. D. Turner, *Automotive sensors*. Momentum Press, LLC, 2009.
- [4] R. Prislan, “Laser Doppler Vibrometry and Modal Testing,” *University of Ljubljana*, Apr. 2008.
- [5] P. Ripka, *Magnetic sensors and magnetometers*. Boston: Artech House, 2001.
- [6] J. Lenz and S. Edelstein, “Magnetic sensors and their applications,” *IEEE Sensors Journal*, vol. 6, no. 3, pp. 631–649, 2006.
- [7] C. Reig, M.-D. Cubells-Beltrán, and D. R. Muñoz, “Magnetic Field Sensors Based on Giant Magnetoresistance (GMR) Technology: Applications in Electrical Current Sensing,” *Sensors*, vol. 9, no. 10, pp. 7919–7942, Dec. 2009.
- [8] J. M. Daughton, “Magnetoresistive Random Access Memory (MRAM),” Feb. 2000.
- [9] “Hall vs. Variable Reluctance Sensors.” Full Function Engineering L.L.C. , 2012.
- [10] G. Carta, D. Hammerschmidt, E. Katzmaier, W. Granig, D. Tatschl, and J. Zimmer, “Giant Magneto Resistors Sensor Technology and Automotive Applications,” 2005.
- [11] J. Pelegri, J. Alberola, R. Lajara, and J. Santiso, “Vibration Detector based on GMR Sensors,” *2007 IEEE Instrumentation & Measurement Technology Conference IMTC 2007*, 2007.
- [12] K. M. Goh, H. L. Chan, S. Ong, W. Moh, D. Tows, and K. V. Ling, “Wireless GMR Sensor Node for Vibration Monitoring,” *2010 5th IEEE Conference on Industrial Electronics and Applications*, 2010.
- [13] Z. S. Tseng , “Undamped One-Dimensional Wave Equation: Vibrations of an Elastic String.”
- [14] J. Gulla and T. Katedralskole, “Modeling the wave motion of a guitar string,” thesis, 2012.
- [15] P. Perov, W. Johnson, and N. Perova-Mello, “The physics of guitar string vibrations,” *American Journal of Physics*, vol. 84, no. 1, pp. 38–43, 2016.

- [16] Z. Mohamad, S. Dixon, and C. Harte, "Pickup position and plucking point estimation on an electric guitar via autocorrelation," *The Journal of the Acoustical Society of America*, vol. 142, no. 6, pp. 3530–3540, 2017.
- [17] N. H. Fletcher, "Plucked Strings – A Review", *Catgut Acoust. Soc. Newsl.* 26, pp. 13–17, 1976.
- [18] J. D. Tillman, "Response effects of guitar pickup position and width", 2002.
- [19] K.-M. H. Lenssen, G. H. J. Somers, and J. B. A. D. Van Zon, "Magnetoresistive sensors for string instruments," *Journal of Applied Physics*, vol. 91, no. 10, p. 7777, 2002.
- [20] C. Atteya, D. Campbell, K. M. S. Oo, and J. M. Vasconcelos, "Giant Magnetoresistance Electric Guitar Pickup," rep.
- [21] "Application Notes for GMR Sensors." [Online]. Available: <https://www.nve.com/Downloads/apps.pdf>.
- [22] *Magnetic Sensors - Development Trends and Applications*. InTech, 2017.
- [23] "AA/AB -Series Analog Magnetic Sensors - NVE." [Online]. Available: https://www.nve.com/Downloads/analog_catalog.pdf.
- [24] J. P. Sebasti a, J. A. Lluch, and J. R. L. Vizca no, "Signal conditioning for GMR magnetic sensors," *Sensors and Actuators A: Physical*, vol. 137, no. 2, pp. 230–235, 2007.
- [25] "TMR Angle Sensors", *Product.tdk.com*, 2018. [Online]. Available: https://product.tdk.com/info/en/products/sensor/angle/tmr_angle/technote/tpo/index.html.